J. Fluid Mech. (2021), *vol*. 912, A18, doi:10.1017/jfm.2020.1092

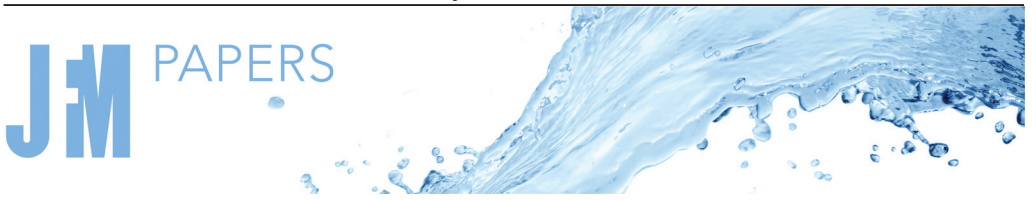

Polymer scission in turbulent flows

Dario Vincenzi[1],†, **Takeshi Watanabe**[2], **Samriddhi Sankar Ray**[3] **and Jason R. Picardo**[4]

[1]Université Côte d'Azur, CNRS, LJAD, 06100 Nice, France

[2]Department of Physical Science and Engineering, Nagoya Institute of Technology, Gokiso, Nagoya 466-8555, Japan

[3]International Centre for Theoretical Sciences, Tata Institute of Fundamental Research, Bangalore 560089, India

[4]Department of Chemical Engineering, Indian Institute of Technology Bombay, Mumbai 400076, India

(Received 28 April 2020; revised 7 November 2020; accepted 1 December 2020)

Polymers in a turbulent flow are subject to intense strain, which can cause their scission and thereby limit the experimental study and application of phenomena such as turbulent drag reduction and elastic turbulence. In this paper, we study polymer scission in homogeneous isotropic turbulence, through a combination of stochastic modelling, based on a Gaussian time-decorrelated random flow, and direct numerical simulations (DNS) with both one-way (passive) and two-way (active) coupling of the polymers, modelled as bead-spring chains, and the flow. For the first scission of passive polymers, the stochastic model yields analytical predictions which are found to be in good agreement with results from the DNS, for the temporal evolution of the fraction of unbroken polymers and the statistics of the survival of polymers. The impact of scission on the dynamics of a turbulent polymer solution is investigated through DNS with two-way coupling (active polymers). Our results indicate that the reduction of kinetic energy dissipation due to feedback from stretched polymers is an inherently transient effect, which is lost as the polymers break up. Thus, the overall dissipation reduction is maximized by an intermediate polymer relaxation time, for which polymers stretch significantly but without breaking too quickly. We also study the dynamics of the polymer fragments which form after scission; these daughter polymers can themselves undergo subsequent, repeated, breakups to produce a hierarchical population of polymers with a range of relaxation times and scission rates.

Key words: polymers, isotropic turbulence

† Email address for correspondence: dario.vincenzi@univ-cotedazur.fr

1. Introduction

The viscoelastic properties of dilute polymer solutions are central to several applications (Larson 1999). When the pure solvent is turbulent the most remarkable effect of the addition of polymers is a significant reduction of the turbulent drag below that of the solvent (Procaccia, L'Vov & Benzi 2008; White & Mungal 2008; Benzi 2010; Graham 2014). This phenomenon, also known as the Toms effect (Toms 1949, 1977), is commonly utilized to reduce the energy losses in pipelines and hence the costs associated with the transport of crude oil. However, in a turbulent flow, polymers are subject to mechanical degradation due to the fluctuating strain rate, which stretches polymers and thus causes their scission. Since turbulent drag reduction decreases with the molecular weight of the dissolved polymers (Virk 1975), the efficacy of polymers as drag reducing agents diminishes in time, with a strong impact on both industrial applications and laboratory experiments (Paterson & Abernathy (1970), Moussa, Tiu & Sridhar (1993), den Toonder *et al.* (1995), Choi *et al.* (2002), Vanapalli, Islam & Solomon (2005), Vanapalli, Ceccio & Solomon (2006), Elbing *et al.* (2009), Pereira & Soares (2012), Owolabi, Dennis & Poole (2017), see also the editorial of Poole (2020) and the review of Soares (2020)).

Analogous mechanical degradation and, by association, practical limitations are observed in experiments of homogeneous and isotropic turbulence with polymer additives (Crawford *et al.* 2008). Indeed, even though in isotropic turbulence the mean strain rate is zero, on average line elements are stretched exponentially at a rate proportional to the inverse of the Kolmogorov dissipation time scale (Bec *et al.* 2006). At large Reynolds numbers, polymers therefore experience strong straining events that can highly distort them. This has been confirmed in experiments and numerical simulations, both directly by examination of the probability distribution of polymer extensions (Vaithianathan & Collins 2003; Vincenzi *et al.* 2007, 2015; Jin & Collins 2008; Watanabe & Gotoh 2010) and indirectly through the observation of a strong polymer feedback on the flow (De Angelis *et al.* 2005; Perlekar, Mitra & Pandit 2006, 2010; Crawford *et al.* 2008; Ouellette, Xu & Bodenschatz 2009; Xi, Bodenschatz & Xu 2013; Watanabe & Gotoh 2013*a*,*b*, 2014; de Chaumont Quitry & Ouellette 2016). Furthermore, experimental measurements of polymer scission in different channel flows, by Vanapalli *et al.* (2006), show that the majority of polymers reside, and therefore break up, in the bulk of the fluid, where the flow approximates isotropic turbulence, rendering the scission results independent of channel geometry.

Mechanical degradation has also been reported in the regime of elastic turbulence (Groisman & Steinberg 2004). Although the Reynolds number of the solution is low in this case, elastic instabilities generate a chaotic flow with highly fluctuating velocity gradients that stretch polymers up to their maximum length (Liu & Steinberg 2014).

A detailed knowledge of the statistics of polymer scission in turbulent flows is thus important for the design of experiments and the performance of realistic simulations of both turbulent drag reduction and elastic turbulence. In laminar flows, considerable progress has been made in the modelling and simulation of polymer scission (e.g. Cascales & de la Torre 1991, 1992; Hsieh, Park & Larson 2005; Sim, Khomami & Sureshkumar 2007; Wu *et al.* 2018). However, the knowledge gained from the study of laminar flows cannot be directly applied to turbulent flows because of the different properties of the strain rate, and consequently of the flow-induced polymer stretching, in the two types of flows. In an extensional velocity field, for instance, the probability distribution of polymer extensions is dominated by a peak that shifts towards larger extensions as the strain rate increases (Perkins, Smith & Chu 1997), and therefore scission is observed only for a sufficiently large strain rate. In contrast, for turbulent flows, the distribution

of the extensions has a wide power-law core due to the intensely fluctuating strain rate (Balkovsky, Fouxon & Lebedev 2000; Watanabe & Gotoh 2010; Liu & Steinberg 2014). Hence the scission rate may be non-negligible even at moderate Reynolds numbers (proportional to the average magnitude of the fluctuating strain rate).

Unlike the fragmentation of liquid jets, sheets, or drops (Villermaux 2007, 2020), the modelling of flow-driven scission in turbulent polymer solutions is still in its infancy (Soares 2020). The reason for this has to be sought in the difficulty of including the microscopic details of the scission process in constitutive models of polymer solutions. To our knowledge, the only continuum model that takes scission into account has been proposed by Pereira, Mompean & Soares (2018) and assumes that the maximum contour length is a spatiotemporal scalar field that decays due to scission while being transported by the fluid. Further development of continuum models requires an in depth understanding of the statistics of scission and the consequent reduction of the relaxation time – in addition to the decrease in the maximum contour length – of the polymer fragments.

We therefore investigate the dynamics of polymers in a three-dimensional homogeneous and isotropic turbulent flow focusing on the scission statistics. A polymer is described as a bead-spring chain in a time-dependent, linear velocity field. This polymer model is known as the Rouse (1953) model and represents one of the most common descriptions of a polymer molecule in a flow (in the case in which only two beads are considered, the Rouse model reduces to the elastic dumbbell model, see Bird *et al.* (1977)). Even when the flow is turbulent, the assumption of a linear velocity field is justified, since the size of polymers is generally smaller than the Kolmogorov dissipation scale η_K, below which viscosity strongly damps the spatial fluctuations of the velocity. We introduce scission into the Rouse model by assuming that the bead-spring chain breaks into two shorter chains as soon as the tension in one of the springs exceeds a critical threshold.

We begin by considering the statistics of the first scission. For passively transported polymers, for which the motion of the polymers does not modify the carrier velocity field, we derive qualitative analytical predictions by restricting ourselves to the Hookean dumbbell model and by using a decorrelated-in-time Gaussian stochastic velocity field (the approach is adapted from a study of droplet breakup conducted in Ray & Vincenzi (2018)). The theoretical predictions are compared with Lagrangian direct numerical simulations (DNS) of the Rouse model in three-dimensional homogeneous isotropic turbulence. We then show that these results are qualitatively insensitive to the introduction of hydrodynamic interactions (HI) and excluded volume (EV) interactions among the beads of the polymer model. For active polymers, the statistics of the first scission is studied via hybrid Eulerian–Lagrangian simulations (Watanabe & Gotoh 2013*a*,*b*, 2014), in which the feedback of (dumbbell-like) polymers onto the velocity field is taken into account. These simulations shed light on the transient nature of the dissipation-reduction effect, which owes its origin to polymer stretching and its demise to polymer scission. Finally, we analyse multiple scissions of passive polymers, via DNS in which a hierarchy of daughter polymers arise from successive breakups, each with their own statistics.

2. The Rouse chain

The Rouse model describes a polymer as a chain of $\mathcal{N}$ inertialess beads connected to their nearest neighbours by elastic springs. We consider finitely extensible nonlinear elastic (FENE) springs with spring constant H and maximum length Q_m. The fluid in which the chain is immersed is Newtonian and its motion is described by an incompressible velocity field $\boldsymbol{u}(\boldsymbol{x}, t)$. The drag force of the fluid on each bead is given by Stokes law with drag coefficient ζ; the collisions of the molecules of the fluid with a bead are described by

Brownian motion. Finally, in the Rouse model, HI and EV interactions between different segments of the chain are disregarded. (These interactions do not affect the scission statistics qualitatively, as shown later in § 3.2.)

The motion of the chain is described in terms of the position of its centre of mass, $\boldsymbol{X}_c$, and the separation vectors between the beads, $\boldsymbol{Q}_i$ ($i = 1, \ldots, \mathscr{N} - 1$). This set of coordinates evolves according to the equations (Bird *et al.* 1977; Öttinger 1996)

$$\dot{\boldsymbol{X}}_c = \boldsymbol{u}(\boldsymbol{X}_c(t), t) + \frac{1}{\mathscr{N}}\sqrt{\frac{Q_{eq}^2}{6\tau}}\sum_{i=1}^{\mathscr{N}} \boldsymbol{\xi}_i(t), \tag{2.1a}$$

$$\dot{\boldsymbol{Q}}_i = \boldsymbol{\kappa}(t)\cdot\boldsymbol{Q}_i(t) - \frac{1}{4\tau}[2f_i\boldsymbol{Q}_i(t) - f_{i+1}\boldsymbol{Q}_{i+1}(t) - f_{i-1}\boldsymbol{Q}_{i-1}(t)] + \sqrt{\frac{Q_{eq}^2}{6\tau}}[\boldsymbol{\xi}_{i+1}(t) - \boldsymbol{\xi}_i(t)], \quad i = 1, \ldots, \mathscr{N} - 1, \tag{2.1b}$$

where $\kappa^{\alpha\beta}(t) = \nabla^\beta u^\alpha(\boldsymbol{X}_c(t), t)$ is the velocity gradient evaluated at the position of the centre of mass, $\tau = \zeta/4H$ is the characteristic time scale of the springs, $Q_{eq} = \sqrt{3k_BT/H}$ is their equilibrium root mean square (r.m.s.) extension (k_B denotes the Boltzmann constant and T is temperature), and $\boldsymbol{\xi}_i(t)$ ($i = 1, \ldots, \mathscr{N}$) are independent, vectorial, white noises. The coefficients

$$f_i = \frac{1}{1 - |\boldsymbol{Q}_i|^2/Q_m^2} \tag{2.2}$$

characterize the FENE interactions and ensure that the extension of each spring does not exceed its maximum length Q_m. Obviously, in the equations for $\boldsymbol{Q}_1$ and $\boldsymbol{Q}_{\mathscr{N}-1}$ it is assumed that $\boldsymbol{Q}_0 = \boldsymbol{Q}_{\mathscr{N}} = 0$.

The end-to-end separation or extension vector of the polymer is defined as $\boldsymbol{R} = \sum_{i=1}^{\mathscr{N}-1}\boldsymbol{Q}_i$. In a still fluid, the equilibrium r.m.s. value of $|\boldsymbol{R}|$ is $r_{eq} = Q_{eq}\sqrt{\mathscr{N} - 1}$ (Bird *et al.* 1977).

We modify the Rouse model in order to account for the scission of the polymer when the tension in any of the springs exceeds a critical value. Since the relation between the tension and the extension of a spring can be easily inverted (Thiffeault 2003), we can, equivalently, assume that for each spring of the chain there exists a critical scission length ℓ_{sc} such that the spring breaks if the length of the corresponding separation vector exceeds ℓ_{sc} (i.e. the chain breaks if $|\boldsymbol{Q}_i| \geqslant \ell_{sc}$ for any $1 \leqslant i \leqslant \mathscr{N} - 1$).

The scission process is non-stationary; the dynamics of the chain therefore depends on its initial configuration and, in particular, on its initial end-to-end separation $r_0 = |\boldsymbol{R}(0)|$. In the following we shall assume that ℓ_{sc} is much greater than $r_0/(\mathscr{N} - 1)$ and that r_0 is equal to r_{eq} or greater than it. (In principle, r_0 could also be taken smaller than r_{eq}, but we have checked that this case does not differ appreciably from the $r_0 \simeq r_{eq}$ one.)

Finally, the size of the chain always remains smaller than η_K, so that the velocity field at the scale of the chain can be considered as linear and the dynamics of the polymer is entirely determined by the velocity gradient at the location of the centre of mass, consistent with the Rouse model.

To summarize, the spatial scales that characterize the system are arranged as follows: $r_{eq} \leqslant r_0 \ll \ell_{sc}(\mathscr{N} - 1) < Q_m(\mathscr{N} - 1) < \eta_K$.

3. First-scission statistics

3.1. *Passive polymers*

3.1.1. *Analytical predictions*

Here we make some simplifying assumptions on both the polymer model and the carrier flow in order to derive analytical predictions for the statistics of polymer scission.

First of all, we only consider the statistics of the first scission. We then restrict ourselves to the $\mathscr{N} = 2$ case, also known as the dumbbell model (Bird *et al.* 1977; Öttinger 1996), i.e. we focus on the slowest deformation mode of the polymer. Many results on single-polymer dynamics in random or turbulent flows have been obtained by using the dumbbell model (see Vincenzi *et al.* (2015) and references therein) and the most common constitutive models of polymer solutions, namely the Oldroyd-B (Oldroyd 1950) and the FENE-P (Bird, Dotson & Johnson 1980) models, are based on it. The legitimacy of this approach is supported by the numerical simulations in Jin & Collins (2008) and Watanabe & Gotoh (2010), where it is shown that, in isotropic turbulence and in the absence of scission, the statistics of the end-to-end separation of a dumbbell and that of an $\mathscr{N} = 20$ chain coincide (provided, of course, that a proper mapping between the parameters of the two systems is applied). Finally, we replace the nonlinear spring with a Hookean one ($f_i = 1$); this is because the nonlinearity of the elastic force enters into play only at extensions close to the scission length, and we shall see from our simulations in § 3.1.2 that it does not affect the qualitative properties of the scission process. For $\mathscr{N} = 2$, (2.1) reduce to

$$\dot{\boldsymbol{X}}_c = \boldsymbol{u}(\boldsymbol{X}_c(t), t) + \frac{1}{2}\sqrt{\frac{r_{eq}^2}{3\tau}}\,\boldsymbol{\zeta}_1(t), \tag{3.1a}$$

$$\dot{\boldsymbol{R}} = \boldsymbol{\kappa}(t)\cdot\boldsymbol{R}(t) - \frac{\boldsymbol{R}(t)}{2\tau} + \sqrt{\frac{r_{eq}^2}{3\tau}}\,\boldsymbol{\zeta}_2(t), \tag{3.1b}$$

where $\boldsymbol{\zeta}_1(t)$ and $\boldsymbol{\zeta}_2(t)$ are (non-independent) vectorial white noises.

We model the flow via the smooth (also known as Batchelor) regime of the Kraichnan (1968) model. This model has been widely employed in the study of turbulent transport (Falkovich, Gawędzki & Vergassola 2001) and has yielded several theoretical results on the coil-stretch transition in random or turbulent flows (see Plan, Ali & Vincenzi (2016) and references therein). The velocity is a divergenceless and spatially smooth Gaussian vector field. It is statistically stationary in time and homogeneous, isotropic, and parity invariant in space; it has zero mean and zero correlation time. Under these assumptions, $\boldsymbol{\kappa}(t)$ is a tensorial white noise with two-time correlation (Falkovich *et al.* 2001)

$$\langle \kappa^{ij}(t)\kappa^{mn}(t')\rangle = \mathscr{K}^{ijmn}\delta(t-t'), \tag{3.2}$$

where

$$\mathscr{K}^{ijmn} = \frac{\lambda}{3}[4\delta^{im}\delta^{jn} - \delta^{ij}\delta^{mn} - \delta^{in}\delta^{jm}] \tag{3.3}$$

and λ is the maximum Lyapunov exponent of the flow. Obviously, the assumption of temporal decorrelation is a strong approximation, since an isotropic turbulent flow has Kubo number $Ku = \lambda t_{corr} \approx 0.6$, where t_{corr} is the correlation time of the flow (Girimaji & Pope 1990; Bec *et al.* 2006; Watanabe & Gotoh 2010). However, it was shown in Musacchio & Vincenzi (2011) that, for a stochastic flow with comparable Ku, the statistics of polymer extension is captured qualitatively by a time decorrelated velocity field.

The Weissenberg number $Wi = \lambda\tau$ determines to what extent polymers are stretched by the flow. In particular, the coil-stretch transition occurs when Wi exceeds the critical value $Wi_{cr} = 1/2$ ((Lumley 1972; Balkovsky *et al.* 2000) – note that our definition of τ and hence that of Wi differ from that of Balkovsky *et al.* (2000) by a factor of 2).

As the velocity field is homogeneous and isotropic in space, the statistics of $R = |\boldsymbol{R}|$ is independent of the position of the centre of mass and of the direction of $\boldsymbol{R}$. To study polymer scission, it is therefore sufficient to focus on the probability density function (p.d.f.) of R, which will be denoted as $P(R, t)$. When $\boldsymbol{\kappa}(t)$ has the properties described above, $P(R, t)$ satisfies the Fokker–Planck equation (Chertkov 2000; Celani, Musacchio & Vincenzi 2005)

$$\partial_{t'} P = \mathbb{L}P, \quad \mathbb{L}P = -\partial_R(D_1 P) + \partial_R^2(D_2 P), \tag{3.4a,b}$$

with rescaled time $t' = t/2\tau$ and coefficients

$$D_1 = \left(\frac{8}{3}Wi - 1\right)R + \frac{2r_{eq}^2}{3R}, \quad D_2 = \frac{2Wi}{3}R^2 + \frac{r_{eq}^2}{3} \tag{3.5a,b}$$

(once again our definition of Wi differs from that used in Chertkov (2000) and Celani *et al.* (2005) by a factor of 2). The appropriate boundary conditions are reflecting at $R = 0$ and absorbing at $R = \ell_{sc}$, i.e.

$$D_1 P - \partial_R(D_2 P) = 0 \quad \text{at } R = 0 \quad \text{and} \quad P(\ell_{sc}, t) = 0 \tag{3.6}$$

for all t. The former condition ensures that the extension of the polymer stays positive, while the latter describes scission at $R = \ell_{sc}$. The analysis of (3.4*a*,*b*) to (3.6) closely follows that in Ray & Vincenzi (2018) for the breakup of sub-Kolmogorov droplets in isotropic turbulence. (The results presented here are deduced directly from those in § 3 of Ray & Vincenzi (2018) by setting $Ca = Wi$, $\mu = 1$, $r_{eq}^2 = Q_{eq}^2/3$, and $f_1(\mu) = f_2(\mu) = \gamma(\mu) = 1$.) We therefore skip the details of the derivations and directly present the predictions of scission statistics.

The number of unbroken polymers that survive at time t, $N_p(t)$, is related to $P(R, t)$ as follows:

$$N_p(t)/N_p(0) = \int_0^{\ell_{sc}} P(R, t)\, \mathrm{d}R. \tag{3.7}$$

At times $t \gg \tau$, $N_p(t)$ therefore decays exponentially as

$$N_p(t) \sim N_p(0)\, \mathrm{e}^{-t/T_d}, \tag{3.8}$$

where the decay time T_d is the reciprocal of the lowest eigenvalue of the operator $\mathbb{L}$ with boundary conditions (3.6). The eigenfunctions of $\mathbb{L}$ are hypergeometric functions with parameters depending on r_{eq}, r_0, Wi and form a discrete set selected by the boundary condition at $R = \ell_{sc}$. A calculation of the lowest eigenvalue shows that T_d depends weakly on Wi for small Wi, decreases rapidly as Wi exceeds Wi_{cr}, and saturates at large Wi.

As we shall see below, the p.d.f. of R integrated over time,

$$\hat{P}(R) = \int_0^{\infty} P(R, t)\, \mathrm{d}t, \tag{3.9}$$

allows us to estimate the mean lifetime of a polymer before its first scission. If the initial distribution of polymer sizes is 'monodisperse', i.e. $P(R, 0) = \delta(R - r_0)$, then $\hat{P}(R)$ takes

the form

$$\hat{P}(R) \propto \begin{cases} \mathrm{e}^{-\Phi(R)}[\phi(\ell_{sc}) - \phi(r_0)] & \text{if } 0 \leqslant R \leqslant r_0, \\ \mathrm{e}^{-\Phi(R)}[\phi(\ell_{sc}) - \phi(R)] & \text{if } r_0 < R \leqslant \ell_{sc} \end{cases} \tag{3.10}$$

with

$$\Phi(R) = \ln D_2(R) - \int^R \frac{D_1(\zeta)}{D_2(\zeta)}\,\mathrm{d}\zeta, \quad \phi(R) = \int^R \frac{\mathrm{e}^{\Phi}(\zeta)}{D_2(\zeta)}\,\mathrm{d}\zeta \tag{3.11a,b}$$

and hence

$$\hat{P}(R) \sim \begin{cases} r_{eq}^{-2} r_0^{-1} R^2 & \text{if } 0 \leqslant R \ll r_{eq}, \\ |r_0^{\alpha} - \ell_{sc}^{\alpha}| R^{-1-\alpha} & \text{if } r_{eq} \ll R \ll r_0, \\ \ell_{sc}^{\beta} R^{-1-\beta} & \text{if } r_0 \ll R \ll \ell_{sc}, \end{cases} \tag{3.12}$$

where $\alpha = 3(Wi^{-1} - 2)/2$ and

$$\beta = \begin{cases} \alpha & \text{if } Wi < Wi_{cr}, \\ 0 & \text{if } Wi > Wi_{cr}. \end{cases} \tag{3.13}$$

Therefore, above the coil-stretch transition, the right-hand tail of $\hat{P}(R)$ saturates to the power-law R^{-1}. An analogous behaviour was found previously for the size distribution of sub-Kolmogorov droplets in isotropic turbulence (Biferale, Meneveau & Verzicco 2014; Ray & Vincenzi 2018). Also note that the exponent α coincides with the one obtained by Balkovsky *et al.* (2000) for the p.d.f. of intermediate extensions in the absence of scission.

If the initial distribution of polymer sizes is broad but nonetheless admits a maximum size r_0, then the left ($R \ll r_{eq}$) and right ($r_0 \ll R \ll \ell_{sc}$) power-law tails continue to exist, but $\hat{P}(R)$ no longer behaves as a power-law for extensions $r_{eq} \ll R \ll r_0$.

The mean time $\langle T_{sc} \rangle$ it takes for a polymer to undergo its first scission can be deduced from the behaviour of $\hat{P}(R)$ via the relation

$$\langle T_{sc} \rangle = \int_0^{\ell_{sc}} \hat{P}(R)\,\mathrm{d}R. \tag{3.14}$$

Equation (3.12) then yields two different behaviours below and above the coil-stretch transition

$$\lambda \langle T_{sc} \rangle \sim \begin{cases} (\ell_{sc}/r_0)^{\beta} & \text{if } Wi < Wi_{cr}, \\ \ln(\ell_{sc}/r_0) & \text{if } Wi > Wi_{cr}. \end{cases} \tag{3.15}$$

3.1.2. *DNS*

In this section, we present numerical simulations of the Rouse model (2.1) in homogeneous and isotropic turbulence and compare them with the analytical predictions of § 3.1.1. The velocity field $\boldsymbol{u}(\boldsymbol{x}, t)$ is the solution of the incompressible Navier–Stokes equations,

$$\partial_t \boldsymbol{u} + \boldsymbol{u} \cdot \boldsymbol{\nabla} \boldsymbol{u} = -\boldsymbol{\nabla} p + \nu_f \Delta \boldsymbol{u} + \boldsymbol{F}, \quad \boldsymbol{\nabla} \cdot \boldsymbol{u} = 0, \tag{3.16a,b}$$

over the periodic cube $[0, 2\pi]^3$. Here p is pressure, ν_f is the kinematic viscosity and $\boldsymbol{F}(\boldsymbol{x}, t)$ is a body force that maintains a constant kinetic energy input ϵ_{in}. The numerical integration uses a standard, fully dealiased pseudo-spectral method with 512^3 collocation points and, for the time evolution, a second-order slaved Adams–Bashforth scheme with

time step $\mathrm{d}t = 4 \times 10^{-4}$. The values of ν_f and ϵ_{in} are such that the Taylor-microscale Reynolds number is $Re_\lambda = 111$. The Lyapunov exponent of the flow is $\lambda = 0.15\tau_\eta^{-1}$, where τ_η denotes the Kolmogorov time scale, consistent with the value found earlier in Bec *et al.* (2006) and Watanabe & Gotoh (2010).

The position of the centre of mass of the polymer is obtained by integrating (2.1*a*) via a second-order Adam–Bashforth method with the same $\mathrm{d}t$ as for the Navier–Stokes equations. The noise term in (2.1*a*) is disregarded, because it has a negligible effect when $\boldsymbol{u}(\boldsymbol{x}, t)$ is turbulent. Moreover, its amplitude is smaller than that of the noise terms in the equations for the separation vectors by a factor of $\mathscr{N}$. As $\boldsymbol{u}(\boldsymbol{x}, t)$ is only known over a discrete grid, the integration of (2.1*a*) requires interpolation to reconstruct the velocity field at $\boldsymbol{X}_c(t)$ – a trilinear scheme is used for this purpose. The same approach allows the calculation of the velocity gradient along the trajectory of the centre of mass, $\boldsymbol{\kappa}(t)$, and hence the integration of (2.1*b*) by means of the Euler–Maruyama method with time step $\mathrm{d}t$. Since in this section we focus on the statistics of the first scission, a chain is removed from the simulation as soon as it breaks according to the criterion discussed above. The time origin for (2.1*b*) ($t = 0$) is taken in the statistically steady state of the carrier turbulent flow, so that the temporal dynamics of polymers is not influenced by the initial transient evolution of $\boldsymbol{u}(\boldsymbol{x}, t)$. Note that, in the present context, it is not necessary to use integration schemes specifically designed to prevent the extension of the links from exceeding Q_m, since the links, by construction, break well before their extension approaches Q_m.

In our simulations, we consider $N_p(0) = 9 \times 10^5$ polymers, whose positions at time $t = 0$ are uniformly distributed in space. Since the statistics of polymer extension depends on the initial size of polymers but not on their orientation, for simplicity the initial condition for the separation vectors is taken to be $\boldsymbol{Q}_i(0) = Q_0(1, 1, 1)/\sqrt{3}$ with $Q_0 > 0$ for all polymers, i.e. the polymers are in a straight configuration and $P(R, 0) = \delta(R - r_0)$ with $r_0 = (\mathscr{N} - 1)Q_0$.

In order to compare chains with different numbers of beads, an appropriate mapping of the chain parameters is needed. We use the mapping proposed by Jin & Collins (2008) and also used by Watanabe & Gotoh (2010). If the parameters of the individual links of an $\mathscr{N}$-bead chain are τ, Q_{eq}, Q_m, ℓ_{sc}, then the statistics of the end-to-end separation of the chain is equivalent to that of a dumbbell with the following parameters:

$$\tau^D = \frac{\mathscr{N}(\mathscr{N}+1)\tau}{6}, \quad Q_{eq}^D = Q_{eq}, \quad Q_m^D = Q_m\sqrt{\mathscr{N}-1}, \quad \ell_{sc}^D = \ell_{sc}\sqrt{\mathscr{N}-1}, \tag{3.17a–d}$$

where the last relation is introduced for compatibility with the expression of Q_m^D. This mapping allows us to compare chains with different numbers of beads by using the dumbbell model as a reference.

Following Watanabe & Gotoh (2010), we define the Weissenberg number for a Rouse chain as $Wi = \lambda\tau^D$. In our simulations, $0.4 \leqslant Wi \leqslant 8$. (Note that small-$Wi$ simulations are computationally more demanding, because the calculation of quantities like $\hat{P}(R)$ and $\langle T_{sc}\rangle$ requires that the time evolution is long enough for all polymers to break, and the time at which the scission process is complete becomes longer and longer as Wi decreases.)

As for the choice of the other parameters, we take $r_{eq} = 1$, $Q_m^D = \sqrt{3000}$ (also following Jin & Collins (2008) and Watanabe & Gotoh (2010)), and, unless otherwise specified, $r_0 = r_{eq}$. In addition, it is assumed that a spring breaks as soon as its extension exceeds $\ell_{sc} = 0.8Q_m$. The number of beads is set to $\mathscr{N} = 10$. We have also performed simulations with different sets of parameters, which support the generality of the results presented below.

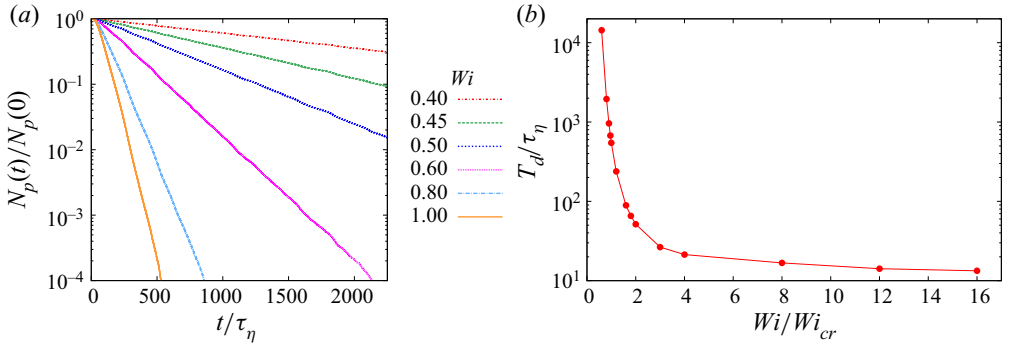

Figure 1. Passive polymers: (*a*) exponential decay of the fraction of unbroken polymers for different values of Wi; (*b*) decay time of the fraction of unbroken polymers rescaled by the Kolmogorov time τ_η as a function of Wi/Wi_{cr}.

It is worth mentioning that the above parameters are compatible with those of the experiment of Crawford *et al.* (2008), which investigates bulk turbulence in a water solution of polyacrylamide (known as PAM) with molecular weight $M_w = 18 \times 10^6$, maximum extension $L = 77\ \mu$m and relaxation time $\tau_p = 43$ ms. Mechanical degradation is observed at $R_\lambda = 485$. For this value of R_λ, the Kolmogorov time scale is reported to be $\tau_\eta = 2.63$ ms, and hence the Weissenberg number based on the Lyapunov exponent can be estimated as $Wi \approx 2.5$.

Figure 1(*a*) shows the temporal evolution of the fraction of unbroken polymers. The decay is exponential with a time scale T_d that decreases rapidly as Wi exceeds its critical value (figure 1*b*), in agreement with the predictions of § 3.1.1. We shall see in § 3.3 that, for a dumbbell, it is possible to write an explicit expression for T_d as a function of Wi.

The time-integrated p.d.f. of the end-to-end extension of unbroken polymers is shown in figure 2(*a*) for an initial polymer size $r_0 = r_{eq}$ and different values of Wi. The p.d.f. displays a power-law behaviour for both $R \ll r_{eq}$ and $r_0 = r_{eq} \ll R \ll \ell_{sc}(\mathcal{N} - 1)$. The left-hand tail is proportional to R^2, because the small separations are dominated by thermal fluctuations. The right-hand tail rises as a function of Wi, until the power-law saturates to R^{-1} for $Wi > Wi_{cr}$. A third power-law emerges for intermediate extensions if $r_0 > r_{eq}$ (figure 2*b*). In this case, the exponent $-1-\alpha$ changes from negative to positive as Wi increases and saturates to 2 at large Wi. To appreciate the coexistence of these three power-laws more clearly, in figure 3*a* we also consider $\hat{P}(R)$ for a much larger value of Q_m^D and a larger separation between r_{eq}, r_0 and $(\mathcal{N} - 1)\ell_{sc}$. All these results confirm the predictions reported in § 3.1.1.

The p.d.f.s presented so far correspond to a 'monodisperse' initial state $P(R) = \delta(R - r_0)$ in which all polymers have the same end-to-end distance. However, as mentioned in § 3.1.1, the behaviour of $\hat{P}(R)$ for intermediate extensions is expected to change if the initial distribution of polymer extensions is broad. To confirm this prediction, we have considered an initial state in which the end-to-end distance of polymers is distributed uniformly between r_{eq} and a maximum initial extension $r_0 > r_{eq}$. The time-integrated p.d.f.s given in figure 3(*b*) show that only the left- and right-hand power-law tails persist in this case, while $\hat{P}(R)$ does not behave as a power-law for intermediate extensions.

We now turn to the statistics of the lifetime T_{sc} of a polymer. The DNS suggest that the p.d.f. of T_{sc} has an exponential tail with a time scale γ^{-1} that, beyond Wi_{cr},

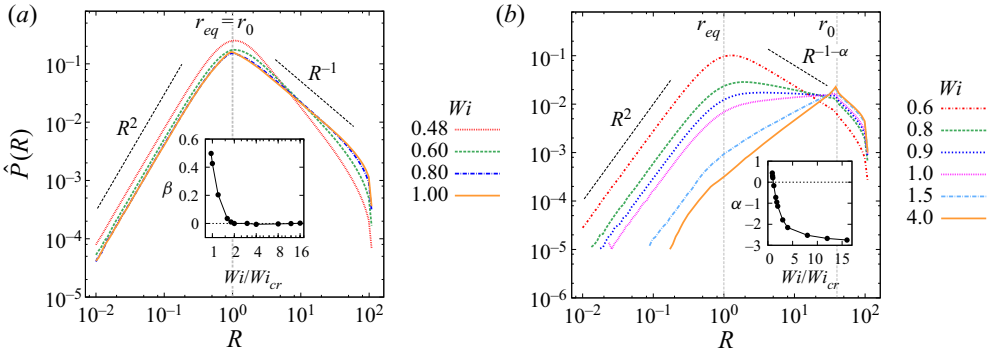

Figure 2. Passive polymers: (*a*) time-integrated p.d.f. of the end-to-end extension of unbroken polymers for $r_0 = r_{eq}$ and for different values of Wi. The inset shows the value of β, which determines the exponent of the right-hand tail of the p.d.f. (i.e. $\hat{P}(R) \propto R^{-1-\beta}$ for $r_0 \ll R \ll \ell_{sc}$), as a function of Wi/Wi_{cr}; (*b*) time-integrated p.d.f. of the end-to-end extension of unbroken polymers for $r_0 = 40 r_{eq}$ and for different values of Wi. The inset shows the value of α, which determines the power-law behaviour of the p.d.f. for intermediate extensions (i.e. $\hat{P}(R) \propto R^{-1-\alpha}$ for $r_{eq} \ll R \ll r_0$), as a function of Wi/Wi_{cr}. In both panels (*a*) and (*b*), the p.d.f.s are normalized to unity for the sake of comparison.

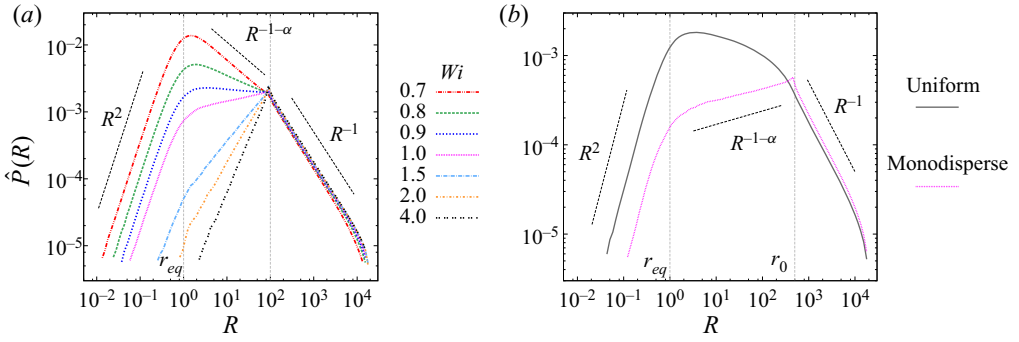

Figure 3. Passive polymers: (*a*) time-integrated p.d.f. of the end-to-end extension of unbroken polymers for $Q_m^D = 10^4$, $r_{eq} = 1$, $r_0 = 10^2$ and different values of Wi; (*b*) time-integrated p.d.f. of the end-to-end extension of unbroken polymers for $Q_m^D = 10^4$, $r_{eq} = 1$, $r_0 = 5 \times 10^2$, $Wi = 1$, and an initial size distribution that is either monodisperse (dotted magenta line) or uniform (between r_{eq} and r_0; solid grey line). In both panels, the p.d.f.s are normalized to unity for the sake of comparison.

decreases rapidly as a function of Wi (figure 4*a*). For all values of the Weissenberg number, γ^{-1} is approximately the same as the decay time T_d of the fraction of unbroken polymers owing to the exponential decay of the latter at long times (see § 3.1.1). However, γ^{-1} differs from $\langle T_{sc} \rangle$, because the exponential behaviour of the p.d.f. of T_{sc} sets in only at relatively large values of T_{sc}. For a fixed Wi, the mean lifetime $\langle T_{sc} \rangle$ behaves as a power of ℓ_{sc}/Q_0 below the coil-stretch transition and as the logarithm of ℓ_{sc}/Q_0 beyond that (see figures 4*b* and 4*c*) – we remind the reader that Q_0 is the initial length of any link of the chain. Small deviations are only observed for $\ell_{sc} \gg Q_0$. Moreover, we have checked that, for $Wi < Wi_{cr}$, the exponent β that gives the dependence of $\langle T_{sc} \rangle$ on ℓ_{sc}/Q_0 is the same as the exponent that describes the right-hand tail of $\hat{P}(R)$, i.e. $\hat{P}(R) \propto R^{-1-\beta}$ for $r_0 \ll R \ll (\mathcal{N} - 1)\ell_{sc}$, in agreement with (3.15). Thus, the statistics of T_{sc} in a turbulent flow is correctly described by the predictions of § 3.1.1.

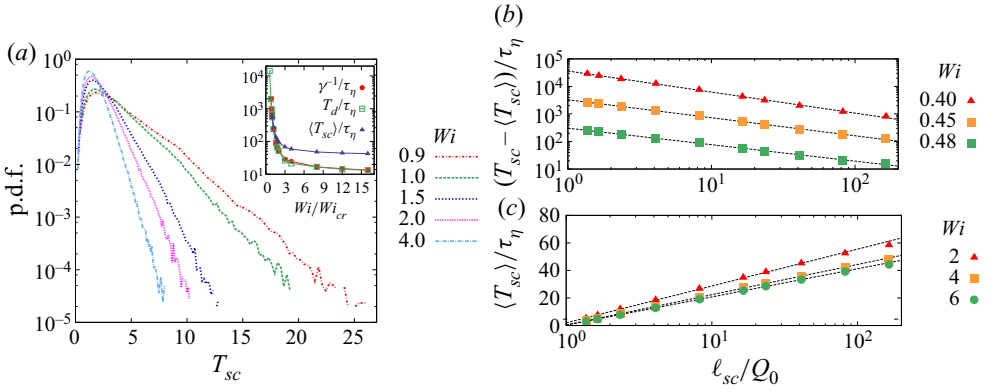

Figure 4. Passive polymers: (*a*) p.d.f. of the lifetime of a polymer for different values of *Wi*. The inset compares the decay time of the fraction of unbroken polymers, the mean lifetime of a polymer and the time scale γ^{-1} in the exponential tail of the p.d.f. ($P(T_{sc}) \sim \mathrm{e}^{-\gamma T_{sc}}$ for $T_{sc}/\tau_\eta \gg 1$) as a function of Wi/Wi_{cr}; (*b*) mean lifetime as a function of ℓ_{sc}/Q_0 below the coil-stretch transition. Here T'_{sc} is a fitting parameter for the dashed lines. The data for $Wi = 0.4$ (respectively, $Wi = 0.45$) are multiplied by a factor of 10^2 (respectively, 10) in order to make the three lines more easily distinguishable; (*c*) the same as in panel (*b*) above the coil-stretch transition.

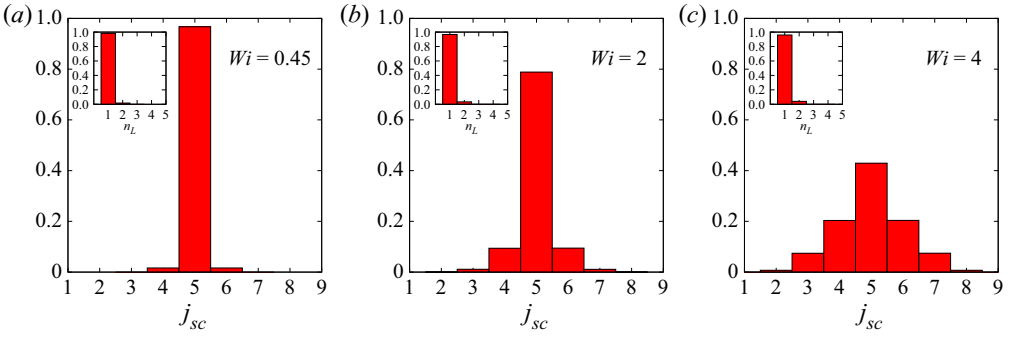

Figure 5. Passive polymers: probability of polymer scission occurring at the j_{sc}-th link for different values of *Wi*. The insets shows the probability of n_L links breaking simultaneously.

We also note that the exponential tail of the distribution of T_{sc} originates from the fact that scission is caused by the cumulative action of the fluctuating strain rate. This is in contrast to the fragmentation of sub-Kolmogorov inextensible fibres, for which the internal tension depends on the instantaneous velocity gradient projected along the fibre. The p.d.f. of the scission time for fibres, therefore, reflects the intermittent statistics of the velocity gradient and is strongly non-exponential (Allende, Henry & Bec 2020).

Figure 5 presents further results on the statistics of the scission process. As previously observed in experiments (Horn & Merrill 1984), scission preferentially happens at the midpoint of the polymer. However, the probability of scission happening at the middle link decreases with *Wi*. The reason for this is that, for small *Wi*, the chain is most of the time in a coiled state and scission occurs because of a sequence of very strong fluctuations of $\boldsymbol{\nabla u}$, whereas for large *Wi* all links are consistently stretched near to the scission length. The insets of figure 5 show that the probability of more than one link breaking simultaneously is generally very small.

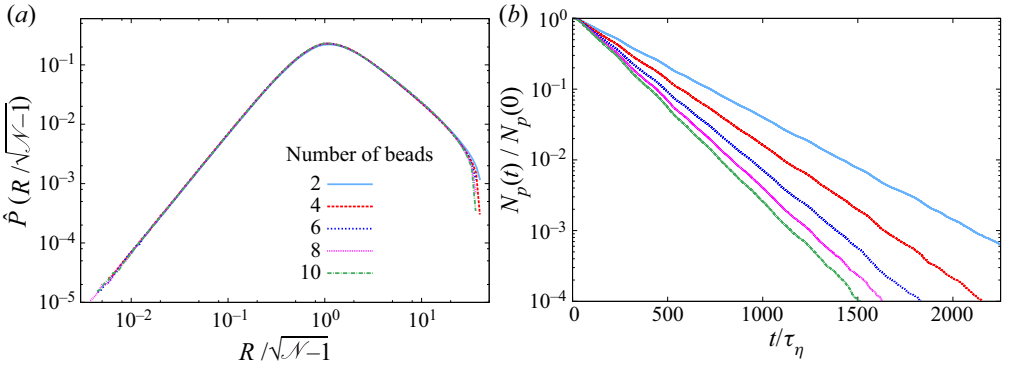

Figure 6. Passive polymers: (*a*) time-integrated p.d.f. of the end-to-end extension of unbroken polymers for $Wi = 0.6$ and different numbers of beads $\mathscr{N}$; (*b*) fraction of unbroken polymers as a function of time for $Wi = 0.6$ and different numbers of beads $\mathscr{N}$.

Finally, it was mentioned in § 3.1.1 that, in the absence of scission, the dumbbell model ($\mathscr{N} = 2$) captures the statistics of the end-to-end extension of a full chain remarkably well, provided the mapping in (3.17*a–d*) is applied (see Watanabe & Gotoh 2010). We have performed an analogous comparison in the presence of scission. The time-integrated p.d.f.s in figure 6(*a*) show that, after the parameters of the chain are suitably rescaled, the time-independent statistics of the end-to-end distance is independent of $\mathscr{N}$, except for small deviations close to the maximum extension. Indeed, for a dumbbell, scission is defined in terms of the end-to-end separation, whereas chains with larger $\mathscr{N}$ break before all the links can stretch up to ℓ_{sc}. These small differences, however, have a significant impact on time-dependent quantities, such as the fraction of unbroken polymers: small-$\mathscr{N}$ chains capture the temporal decay qualitatively, but underestimate the scission rate (see figure 6*b*). The results also suggest that the discrepancies between chains with $\mathscr{N} - 1$ and $\mathscr{N}$ beads diminish as $\mathscr{N}$ increases (figure 6*b*) as well as when *Wi* increases (not shown). We conclude that it is important to consider the dynamics of a full bead-spring chain in order to accurately describe the scission process and achieve quantitative agreement between experiments and models of polymer solutions.

3.2. *Effect of hydrodynamic and excluded volume interactions*

When modelling the rheological properties of dilute polymer solutions, it is important to include HI between the beads of the Rouse model in order to capture effects such as the dependence of solution viscosity on the molecular weight and strain rate, and a non-zero second normal stress difference (Öttinger 1996). However, HI have no qualitative impact on the stretching dynamics of individual polymers in laminar flows (Jendrejack, de Pablo & Graham 2002; Schroeder, Shaqfeh & Chu 2004). Moreover, these forces weaken as a polymer is stretched so that elongated polymers are nearly unaffected by HI (Stone & Graham 2003). This is also true for EV interactions (Cifre & de la Torre 1999; Stone & Graham 2003). Thus, we expect the qualitative nature of scission statistics to be unaffected by both HI and EV forces. Indeed, this has been demonstrated for polymers with HI in laminar flows (Cascales & de la Torre 1991; Knudsen, Hernández Cifre & García de la Torre 1996; Sim *et al.* 2007), where the only effect of HI is a quantitative decrease in the scission rate.

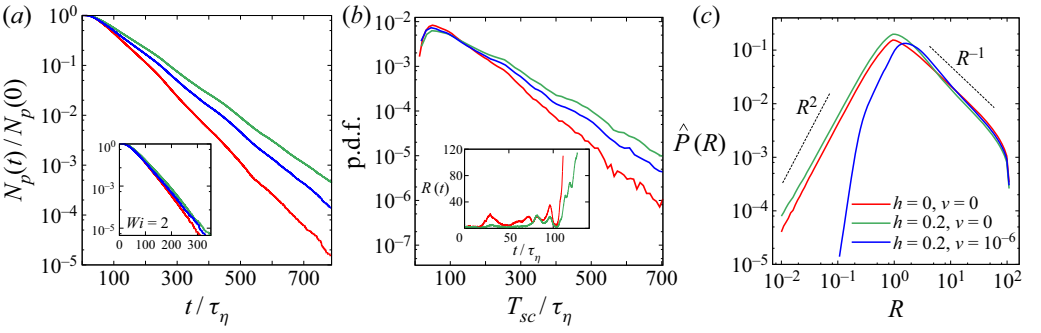

Figure 7. Passive polymers with HI and EV: comparison of the scission statistics for polymers without HI and EV ($h = 0$, $\nu = 0$), with only HI ($\nu = 0$), and with HI and EV (legend in panel (c)). In all three cases $Wi = 0.9$. Panel (a) presents the decay of the fraction of unbroken polymers, with its inset showing the corresponding results for a larger value of $Wi = 2.0$. Panel (b) presents the distribution of lifetimes T_{sc}, while its inset compares typical time traces of the end-to-end extension of polymers with and without HI. Panel (c) shows the time-integrated p.d.f. of the end-to-end extension.

All the studies mentioned above, however, have been conducted in non-turbulent flows. Therefore, it is important to check whether the effects of HI and EV forces on polymer scission remain purely quantitative even in turbulent flows. Towards this end, we modify the model in § 2 to incorporate both HI and EV forces, as described in appendix A. This introduces two non-dimensional parameters, h (related to the bead radius) and ν, which determine the magnitude of the HI and EV forces, respectively. Setting these parameters to zero recovers the Rouse model of § 2.

Our DNS calculations for these HI + EV chains (with $\mathcal{N} = 10$ beads) show that, while the scission statistics remain qualitatively the same, the scission rate is decreased by HI while it is increased by EV forces. These effects are clearly demonstrated by figures 7(a) and 7(b), which depict the evolution of the fraction of surviving polymers and the distribution of polymer lifetimes, respectively. These figures present results for $Wi = 0.9$ for three cases: without HI and EV (red), with only HI (green) and with HI and EV (blue). The decay of the number of unbroken polymers, as well as the distribution of lifetimes, remains exponential in nature even after including HI and EV interactions. However, the scission rate clearly reduces when HI are included and then increases again once EV are also considered. Thus, HI and EV effects oppose each other, reducing their overall impact.

The effects of HI and EV forces diminish as Wi is increased, as shown by the inset of figure 7(a), which presents the evolution of the number of unbroken polymers for a larger value of the Weissenberg number ($Wi = 2$) than the main panel. This occurs because polymers stretch out with increasing ease as Wi increases, while both HI and EV forces are significant only when polymers are coiled and have small extensions. The impotence of these forces, especially EV, at large extensions is reinforced by figure 7(c) which presents the time-integrated p.d.f. of polymer extension for all three cases. The three curves are seen to nearly overlap at large extensions, with significant differences arising only for $R \lesssim R_{eq}$. Indeed, HI and EV affect the scission rate by modifying the initial stretching dynamics of small coiled polymers. The HI are known to inhibit and delay the uncoiling of a coiled polymer in laminar flows (Sim *et al.* 2007). We find that this is true even in a turbulent flow, as illustrated by the inset of figure 7(b) which compares two typical time traces of the end-to-end extension for polymers with and without HI. Thus, HI typically increase the time it takes for a polymer to reach large extensions and thereby reduce the scission

rate in an ensemble of polymers. The EV interactions, in contrast, promote the elongation of a coiled polymer and thus hasten its scission. The dynamics near the scission event, however, are unaffected by HI and EV forces, and we therefore find that the distribution of broken link locations (not shown) remains the same as that for Rouse chains (cf. figure 5).

Having seen that HI and EV interactions have no qualitative impact on the scission statistics, we disregard them in the subsequent sections, wherein the computational burden increases significantly due to either the inclusion of polymer feedback onto the flow or the tracking of broken polymer fragments as they undergo repeated scissions.

3.3. *Active polymers*

We now investigate the implications of the results obtained so far for the two-way-coupling regime in which polymers perturb the surrounding flow.

When polymers break, their effective relaxation time τ^D decreases according to (3.17*a–d*) and the solution, at any point in time, consists of polymers with different τ^D. We can then introduce a mean Weissenberg number $\langle Wi\rangle(t)$, which is defined as the average of $\lambda\tau^D$ over all polymers that compose the solution at time t. Studying the evolution of $\langle Wi\rangle(t)$, in a one-way-coupling simulation, helps us foresee how the effect of polymer feedback on the flow would decay due to scission.

Let us, for the sake of simplicity, consider the case of dumbbells ($\mathcal{N} = 2$) and take an initial ensemble of $N_p(0)$ dumbbells with Weissenberg number Wi_0. When a dumbbell breaks it forms two beads which formally have zero Weissenberg number. Thus, at time t, the system consists of $N_p(t)$ dumbbells with $Wi = Wi_0$ and $2[N_p(0) - N_p(t)]$ single beads with $Wi = 0$. Hence, for an ensemble of dumbbells,

$$\langle Wi\rangle(t) = \frac{N_p(t)}{2N_p(0) - N_p(t)} Wi_0. \tag{3.18}$$

The temporal evolution of $\langle Wi\rangle$ is obtained by calculating $N_p(t)$ from the Lagrangian database used in § 3.1.2 and is shown in figure 8(*a*) for different values of $Wi_0 > Wi_{cr}$. Dumbbells with larger Wi_0 have a larger scission rate, and therefore $\langle Wi\rangle$ vanishes rapidly. In contrast, dumbbells with smaller Wi_0 break relatively slowly and the mean Wi of the solution remains non-zero for a longer time. We note, *en passant*, that $\langle Wi\rangle$ becomes approximately equal to Wi_{cr} at $t \approx 50\tau_\eta$ for all Wi_0. By substituting (3.8) into (3.18), we thus deduce the following empirical expression for the scission rate of dumbbells (see figure 8*b*):

$$\frac{\tau_\eta}{T_d} \propto \ln\left[\frac{1}{2}\left(1 + \frac{Wi}{Wi_{cr}}\right)\right]. \tag{3.19}$$

The behaviour of $\langle Wi\rangle$ shown in figure 8(*a*) suggests that a large value of Wi_0 will produce a polymer feedback that is initially strong but short-lived, decaying rapidly due to scission. In contrast, a moderate value of Wi_0 yields a feedback that, albeit weaker, should last for a longer time and may therefore be more effective.

To investigate this point in a two-way-coupling simulation, we take the hybrid Eulerian–Lagrangian approach proposed by Watanabe & Gotoh (2013*a*,*b*, 2014), which consists in seeding the fluid with a large number of FENE dumbbells and calculating the reaction force exerted by the dumbbells upon the fluid. This amounts to adding the term $\boldsymbol{\nabla} \cdot \boldsymbol{T}_p$ to the right-hand side of the Navier–Stokes equations (3.16*a*,*b*), where $\boldsymbol{T}_p$ is the

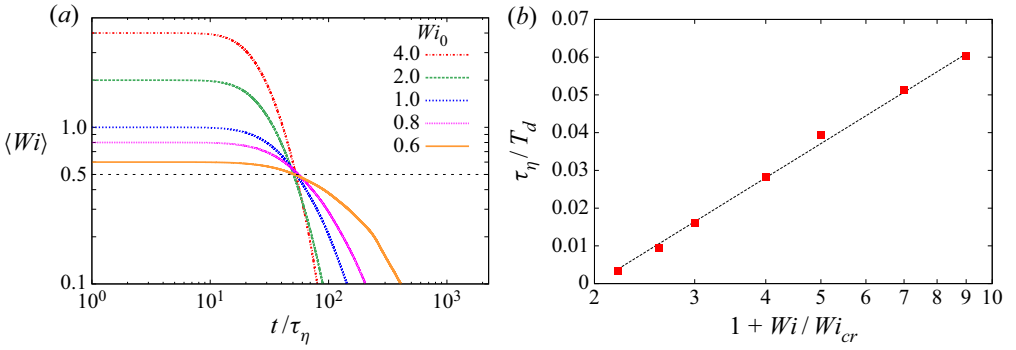

Figure 8. Passive polymers: (*a*) mean Weissenberg number as a function of time for $\mathscr{N} = 2$ and different values of Wi_0; (*b*) reciprocal of T_d (multiplied by the Kolmogorov time scale) as a function of $1 + Wi/Wi_{cr}$. The dashed line is proportional to $\ln[(1 + Wi/Wi_{cr})/2]$.

polymeric contribution to the stress tensor,

$$\boldsymbol{T}_p = \frac{\nu_f \eta L^3}{N_p(0)} \sum_{n=1}^{N_p(0)} \frac{1}{\tau^{(n)}} \left[f\left(\frac{R^{(n)}}{Q_m^D} \right) \frac{3\boldsymbol{R}^{(n)} \otimes \boldsymbol{R}^{(n)}}{r_{eq}^2} - \boldsymbol{I} \right] \delta\left(\boldsymbol{x} - \boldsymbol{X}_c^{(n)} \right). \tag{3.20}$$

In the expression for $\boldsymbol{T}_p$, L is the linear size of the domain and η is the ratio of the polymer to the solvent contribution to the total viscosity of the solution (η is proportional to the volume fraction of dumbbells). The vectors $\boldsymbol{X}_c^{(n)}$ and $\boldsymbol{R}^{(n)}$ are the positions of the centre of mass and the end-to-end separation of the n-th dumbbell, respectively, $\boldsymbol{I}$ is the identity matrix and

$$\frac{1}{\tau^{(n)}} = \begin{cases} \tau^{-1} & \text{for } t < t_{sc}^{(n)} \\ 0 & \text{for } t \geqslant t_{sc}^{(n)}, \end{cases} \tag{3.21}$$

where $t_{sc}^{(n)}$ is the smallest time such that $R^{(n)} = \ell_{sc}$. Thus, the dumbbells stop affecting the velocity field after breaking. The evolution of the position and the configuration of each dumbbell is given by (3.1).

The computational domain is a three-dimensional periodic box with $L = 2\pi$. A pseudo-spectral method with 128^3 grid points and the second-order Runge–Kutta algorithm are used for the integration of the Navier–Stokes equations in space and in time, respectively. The equation for the dumbbells is solved by using the Euler–Maruyama scheme. The turbulent flow is maintained by a forcing with Fourier transform $\hat{\boldsymbol{F}}(\boldsymbol{k}, t) = A(t)\hat{\boldsymbol{u}}(\boldsymbol{k}, t)$ for $1 \leqslant |\boldsymbol{k}| \leqslant 2$ and zero otherwise, where $A(t)$ is such that the kinetic energy input rate ϵ_{in} is constant. We take $\epsilon_{in} = 0.5$ and $\nu_f = 0.015$, which yields $Re_\lambda = 51$ in the absence of polymer feedback (for more details on the simulation, the reader is referred to Watanabe & Gotoh (2013*a*)).

We first evolve the velocity field alone with $\eta = 0$ and then, once a statistically steady flow is obtained, we disperse $N_p(0) = 4 \times 10^8$ polymers with $\eta = 4 \times 10^{-2}$ into the fluid. The time at which the polymers are added to the flow is marked as $t = 0$. As in § 3.1, $Q_m^D/r_{eq} = \sqrt{3000}$, $\ell_{sc} = 0.8Q_m^D$ and $r_0/r_{eq} = 1$. We shall consider three values of the Weissenberg number, $Wi = \lambda\tau = 0.6, 0.8, 1.0$, where λ is the Lyapunov exponent of the Newtonian flow. A set of one-way-coupling simulations ($\eta = 0$), at the same values of Wi, are also performed for comparison.

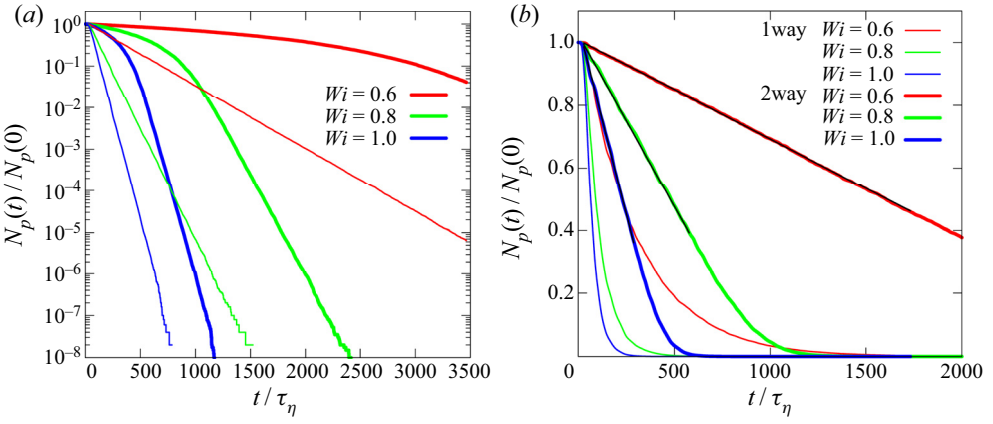

Figure 9. Active polymers: (*a*) fraction of unbroken polymers as a function of time on a semilogarithmic scale. The thin curves refer to the passive simulations ($\eta = 0$), while the thick curves refer to the active ones ($\eta = 4 \times 10^{-2}$). Panel (*b*) is a close-up of the initial decay of the fraction of unbroken polymers on a linear scale. The black lines are $1 - k(t - t_\star)$ with $t_\star/\tau_\eta = 23$ and $k\tau_\eta \times 10^3 = 0.315, 1.10, 2.41$ for $Wi = 0.6, 0.8, 1.0$, respectively.

We begin by examining the time evolution of $N_p(t)/N_p(0)$, which is depicted in figure 9(*a*), for both active (thick lines) and passive (thin lines) polymers. We see that, with polymer feedback, scission proceeds in two stages: (i) an early-time regime in which active polymers break up much slower than passive polymers, and the fraction of unbroken active polymers decays linearly rather than exponentially; and (ii) a long-time regime in which active polymers show the same exponential decay as passive polymers. The initial linear-decay regime is more clearly visible in figure 9(*b*), wherein straight lines (black) of the form $1 - k(t - t_\star)$ provide an excellent fit for the early-time active polymer data. Increasing Wi is seen to increase the linear decay rate k (cf. caption of figure 9), as well as hasten the onset of the exponential decay regime.

This behaviour is a consequence of the way the feedback of an ensemble of polymers evolves as a result of scission. In isotropic turbulence, the dispersion of polymers into a Newtonian solvent reduces the fluid dissipation rate by a factor proportional to the polymer concentration (De Angelis *et al.* 2005; Kalelkar, Govindarajan & Pandit 2005; Perlekar *et al.* 2006; Ouellette *et al.* 2009; Perlekar *et al.* 2010; Watanabe & Gotoh 2013*a*). The time series of the instantaneous fluid dissipation rate

$$\epsilon(t) = \frac{\nu_f}{L^3} \int_{[0,L]^3} |\nabla \boldsymbol{u}(\boldsymbol{x}, t)|^2 \, \mathrm{d}\boldsymbol{x} \tag{3.22}$$

is shown in figure 10, along with the polymer dissipation rate

$$\epsilon_p(t) = \frac{1}{L^3} \int_{[0,L]^3} \boldsymbol{T}_p(\boldsymbol{x}, t) : \boldsymbol{S}(\boldsymbol{x}, t) \, \mathrm{d}\boldsymbol{x}, \tag{3.23}$$

where $\boldsymbol{S}$ is the strain tensor. (Note that under statistically stationary conditions, we would have $\epsilon_{in} = \overline{\epsilon(t)} + \overline{\epsilon_p(t)}$, where the overbar denotes the time averaged value.) At short times, the polymer feedback is fairly strong and causes a significant reduction of $\epsilon(t)$ (and a corresponding increase of $\epsilon_p(t)$) compared with the value for the Newtonian flow. The reduction of $\epsilon(t)$ is associated with a decrease in the amplitude of the velocity gradient and hence entails weaker polymer stretching and a lower probability of scission. For this

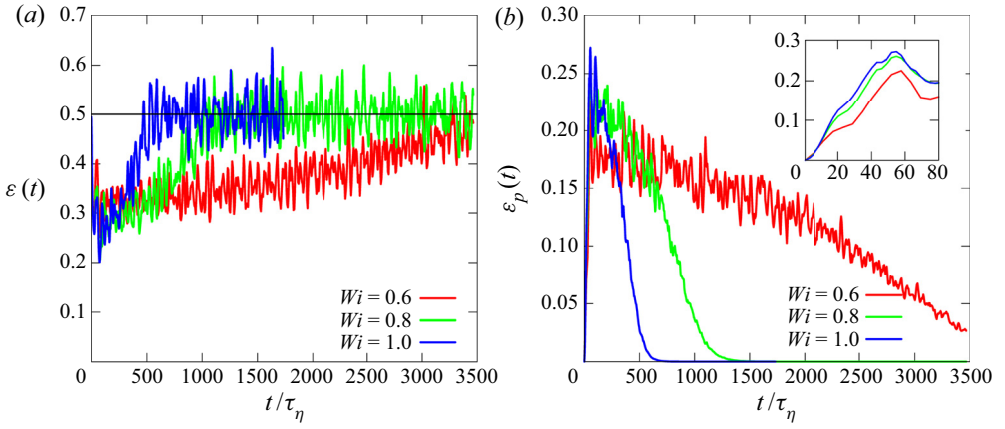

Figure 10. Active polymers: (*a*) fluid and (*b*) polymer dissipation rates as a function of time for different values of *Wi*. The horizontal line in panel (*a*) represents ϵ_{in}, which is the time-averaged value of the fluid dissipation for the Newtonian fluid. The inset in panel (*b*) is a close-up of the main plot over the initial stage of the evolution.

reason, the scission rate is initially small. As time progresses, however, the concentration of unbroken polymers keeps decreasing, until the effect of polymers on the flow becomes negligible and $\epsilon(t)$ returns to its Newtonian value (along with $\epsilon_p(t)$ going to zero). This is accompanied by a growth of the velocity gradient and thus a faster decay of the fraction of unbroken polymers. The fact that the exponential decay regime of active polymers matches that of passive polymers (cf. figure 9) implies that the local feedback of an individual polymer onto the flow in its immediate vicinity does not affect its scission statistics. It is only the combined feedback by all polymers (which is concentration dependent) that can modify scission statistics, by effecting a global change in the dissipation rate of the flow.

Since polymers break more easily for higher values of *Wi*, the time needed for the polymer feedback to vanish decreases with increasing *Wi*. So for $Wi = 1$, while the reduction of energy dissipation is initially stronger, the return to the Newtonian regime is faster; for $Wi = 0.6$ scission proceeds extremely slowly and the dissipation reduction, albeit smaller, lasts for a much longer time.

One important consequence of this analysis is that, for a given experiment, an optimal, not necessarily very large, value of *Wi* exists that maximizes the energy-dissipation reduction integrated over the duration of the experiment.

4. Multiple-scission statistics

We now return to passive polymers and examine how a population evolves when polymers can undergo multiple, repeated scissions. When a polymer chain composed of several beads undergoes its first scission (whose statistics was analysed in § 3.1), it results in two daughter polymers, each containing a smaller number of beads. These daughter polymers can themselves undergo further scissions to produce a tertiary generation, and so on, until, in case of complete breakage, we are left with only individual beads which represent small, inextensible polymer fragments. In this section, we study how this hierarchy of daughter polymers evolves, owing to multiple breakups of the parent polymers. After every scission event, we discard the broken link, form two new daughter polymers, and then follow their evolution along the trajectories of their respective centres of mass, which typically separate exponentially in time due to the positive Lyapunov exponent of the turbulent flow.

In the simulations for first-scission statistics, described earlier in § 3.1.2, we treated the centre of mass and the separation vectors of the polymer chains as the dynamical variables. This formulation becomes inconvenient when dealing with multiple scissions, because new trajectories would have to be spawned after each scission event. So, instead, we adopt the following approach. Consider $N_p(0)$ parent polymer chains, each of which is composed of $\mathscr{N}_0$ beads. Thus, the total number of beads in the simulation, which remains constant in time, is $N_b = \mathscr{N}_0 N_p(0)$. We assign to the beads distinct labels from 1 to N_b and follow the time evolution of their positions. In addition, we maintain an array which records the labels of the first and last beads of every polymer chain in the simulation. So when a polymer chain undergoes a scission, we simply update this array: the broken chain is assigned all the beads preceding the broken link (and thereby becomes the first daughter polymer), while the remaining beads are assigned to a new entry in the array (to form the second daughter polymer). This procedure allows us to simulate the growing population of polymer chains without increasing the number of dynamical variables. For a given chain with $\mathscr{N}$ beads, we still use (2.1) to evolve its dynamics, by calculating $\boldsymbol{X}_c$ and $\boldsymbol{Q}_i$ from the position vectors of the beads, $\boldsymbol{X}_1, \ldots, \boldsymbol{X}_{\mathscr{N}}$ as follows:

$$\boldsymbol{X}_c = \sum_{i=1}^{\mathscr{N}} \boldsymbol{X}_i \quad \text{and} \quad \boldsymbol{Q}_i = \boldsymbol{X}_{i+1} - \boldsymbol{X}_i \ (1 \leqslant i \leqslant \mathscr{N} - 1). \tag{4.1a,b}$$

All other aspects of these simulations follow the description given for the first-scission simulations in § 3.1.2, except that we now simulate the turbulent flow with a more moderate value of $Re_\lambda = 90$, by using 256^3 collocation points and a time step of $\mathrm{d}t = 10^{-3}$. The reason for this is that multiple-scission simulations require the polymers to be evolved simultaneously along with the flow (whereas a precomputed set of Lagrangian trajectories were used to obtain all first-scission statistics), thus necessitating a new flow computation for each variation of the polymer parameters.

At time $t = 0$, the parent polymers are composed of $\mathscr{N}_0$ beads. As a result of scissions, at later times polymers with different numbers of beads will be found in the flow. We thus denote by $N_P(t, \mathscr{N})$ the number of polymers that, at time t, are composed of $\mathscr{N}$ beads.

We begin by examining how $N_P(t, \mathscr{N})$ evolves due to the repeated scission of an initial population of $N_P(0, \mathscr{N}_0)$ parent polymer chains, each with $\mathscr{N}_0 = 10$ beads. Figure 11 presents results for various values of the parent-polymer Weissenberg number, $Wi_0 =$ (*a*) 0.8, (*b*) 1.0, (*c*) 2.0 and (*d*) 4.0. Each $\mathscr{N}$-bead parent/daughter polymer is represented by a different curve, as indicated in the legend. We observe that for the small values of Wi_0 in figure 11(*a*,*b*), only 10-bead polymers break. As shown in figure 5, most of the daughter polymers have five beads (along with a few non-5-bead polymers due to rare off-centre scissions), because scission typically occurs at the central link for small Wi_0. For the larger values of Wi_0 in figure 11(*c*,*d*), the daughter polymers also undergo scissions and the population is eventually dominated by small polymers and individual beads (inextensible polymer fragments).

Clearly, the extent to which polymers can undergo repeated scissions depends on the Wi_0 of the parent polymers. This is because each subsequent scission produces daughter polymers with a smaller relaxation time, which can be quantified by using (3.17*a*) to calculate the effective Weissenberg number of the $\mathscr{N}$-bead daughter polymer

$$Wi = \frac{\mathscr{N}(\mathscr{N}+1)}{\mathscr{N}_0(\mathscr{N}_0+1)} Wi_0, \tag{4.2}$$

where $2 \leqslant \mathscr{N} < \mathscr{N}_0$, and Wi_0 is the Weissenberg number of the parent polymer with $\mathscr{N}_0$ beads. Note that $Wi \equiv 0$ for individual beads ($\mathscr{N} = 1$). An approximate condition for

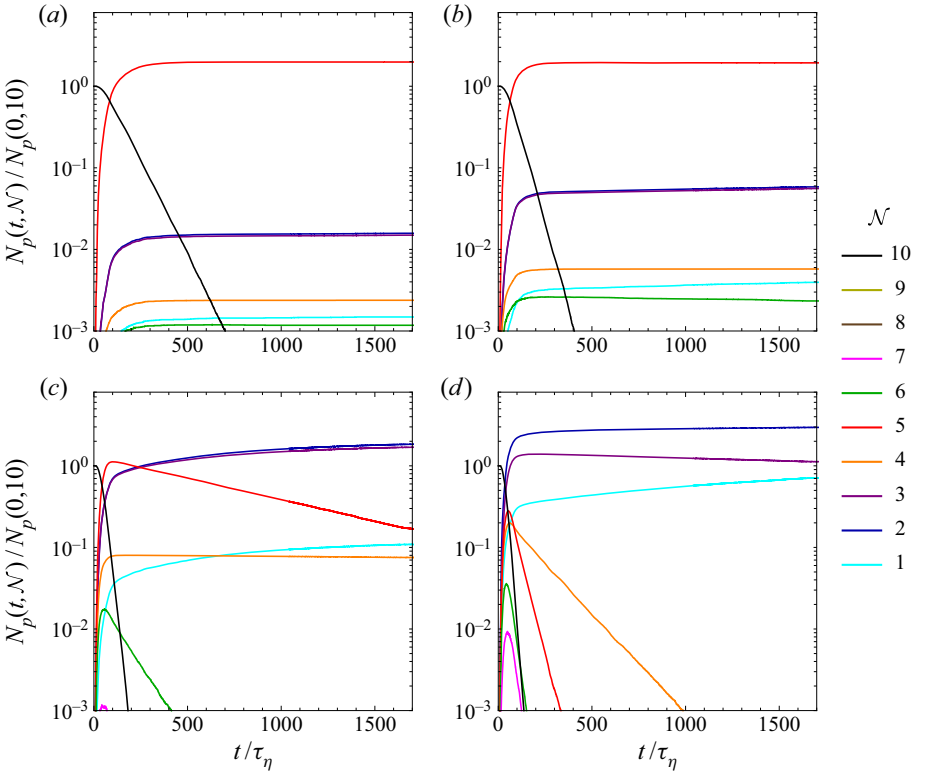

Figure 11. Passive polymers undergoing multiple scissions: evolution of the number of polymers, $N_P(t, \mathcal{N})$, categorized according to the number of constituent beads $\mathcal{N}$, due to the repeated scission of $N_P(0, 10)$ 10-bead parent polymers with (*a*) $Wi_0 = 0.8$, (*b*) $Wi_0 = 1.0$, (*c*) $Wi_0 = 2.0$ and (*d*) $Wi_0 = 4.0$.

a significant fraction of any given generation of daughter polymers to breakup is $Wi > Wi_{cr} = 1/2$. So, if $\mathcal{N}_0 = 10$, (4.2) implies that 5-bead daughter chains will not break up, unless $Wi_0 > 1.83$. The results in figure 11 agree with this estimate: 5-bead daughters experience a slow rate of scission for $Wi_0 = 2.0$ (figure 11*c*), but no scission at all for $Wi_0 = 0.8$ and 1.0 (panels (*a*) and (*b*), respectively). Furthermore, for $Wi_0 = 4.0$, (4.2) leads us to expect scissions of daughter polymers that have $\mathcal{N} = 4$ beads ($Wi = 8/11 > 1/2$) or more, but certainly not if they are composed of only two beads ($Wi = 12/55 < 1/2$). This is exactly what we observe in figure 11(*d*). Thus, the condition $Wi > Wi_{cr}$, in conjunction with (4.2), provides a simple way of estimating the number of beads of the smallest polymer that can be formed by repeated scissions, given Wi_0.

Panels (*c*) and (*d*) of Figure 11 show that the evolution of the number of daughter polymers typically have two regimes. First, there is an enrichment phase, during which daughter polymers are formed due to the rapid breakup of the 10-bead parent polymer. Daughter polymers with various numbers of beads can be formed, especially at large Wi for which off-centre breakups are quite frequent (figure 5). An exponential decay phase then appears for the daughter polymers that have enough beads to undergo further scission, e.g. $\mathcal{N} = 7, 6, 5, 4$ in figure 11(*d*). These secondary breakups produce a second phase of mild enrichment for the smallest polymers that do not break up, e.g. $\mathcal{N} = 2$ in figure 11(*c*,*d*).

The decay time T_d of the number of daughter polymers, in the exponential decay regime, is larger for smaller $\mathcal{N}$, as evidenced by the shallower slopes of the corresponding curves

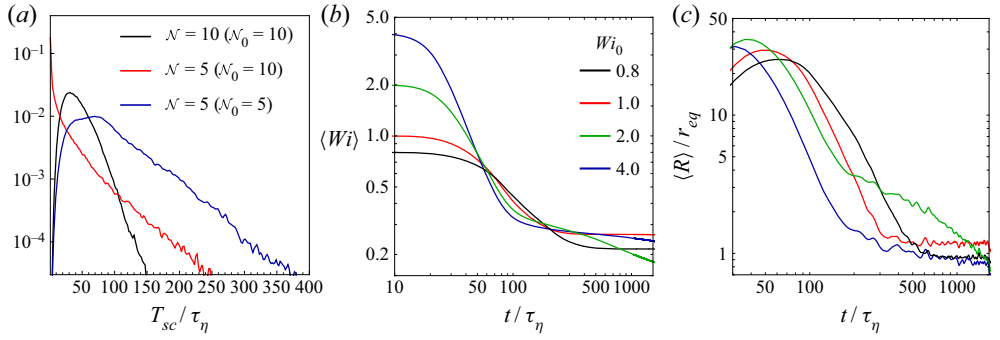

Figure 12. Passive polymers undergoing multiple scissions: (*a*) probability distributions of the lifetime of a parent 10-bead polymer, a daughter 5-bead polymer formed because of the scission of a 10-bead polymer ($\mathcal{N}_0 = 10$) and a parent 5-bead polymer ($\mathcal{N}_0 = 5$) with same $Wi_0 = 4$; (*b*) decay of Wi, averaged over the entire population of polymers, for various values of the initial Wi_0 of the 10-bead parent polymers; (*c*) evolution of the averaged end-to-end extension $\langle R \rangle$ of the polymers for various Wi_0 of the parent polymers.

(e.g. $\mathcal{N} = 7, 6, 5, 4$ in panel (*d*)). This variation follows from figure 1(*b*), provided that the decay time of each daughter polymer can be estimated from figure 1(*b*) by using (4.2) to calculate Wi. However, the use of figure 1(*b*) for daughter polymers is permissible only if the scission kinetics of an $\mathcal{N}$-bead daughter polymer is the same as the first-scission kinetics of a parent polymer that starts with $\mathcal{N}$ beads. To check if this is the case, we ran a separate simulation to calculate the distribution of survival times of 5-bead parent polymers ($\mathcal{N}_0 = 5$, $\mathcal{N} = 5$). In figure 12(*a*), this result (blue) is compared with the survival time distribution of 5-bead daughter polymers (red), which form due to the breakup of 10-bead parent polymers. The corresponding distribution for the 10-bead parent polymers (black) is also shown for comparison. Remarkably, we see that daughter polymers have a much higher probability of breaking at early times than parent polymers with the same number of beads. This is because daughter polymers are formed from scission events: they typically start out in a stretched configuration and so have a much higher probability of breaking quickly than a randomly initialized, coiled parent polymer with the same number of beads. The effect of this fades quite quickly, though, and for times larger than the Lagrangian decorrelation time $T_L \approx 10\tau_\eta$ (for $Re_\lambda \sim 10^2$; see Yeung (2002)) the survival time p.d.f. of the daughter polymers begins to resemble that of the parent polymers with the same number of beads. The time scales associated with the two exponential tails are, therefore, approximately the same, and one can indeed estimate the long-term decay time scale (or equivalently the decay rate) of an $\mathcal{N}$-bead daughter polymer, formed due to multiple scissions, by using just the first-scission statistics of a parent polymer with the same number of beads.

Can the early-time, high scission probability of daughter polymers be ignored? This depends on the Wi of the daughter polymers. From figure 1(*b*), we expect $T_d \gg T_L$ for small $Wi \lesssim 1$; the number of polymers that would break up during the initial time T_L will then be relatively small, and may be ignored. However, for larger $Wi \gtrsim 4$, we have $T_d \approx T_L$ and a significant fraction of daughter polymers would break before they forget their stretched initial conditions. Therefore, for large Wi_0 (which would produce daughter polymers with large Wi), it becomes important to simulate multiple scissions in order to faithfully describe the decay of the polymer population. Such simulations would have to be repeated if the number of beads of the parent polymer changes. The situation simplifies considerably, however, for small Wi_0 as one can then use first-scission statistics,

calculated for a range of $\mathscr{N}$, to describe the decay of daughter polymers, regardless of the number of beads of the parent polymer.

The evolution of Wi averaged over all polymers, which represents the mean effective Wi of the entire population, is shown in figure 12(b), for various values of Wi_0 of the parent polymers. This is the analogue of figure 8(a), but for $\mathscr{N}_0 = 10$ rather than 2. We see that $\langle Wi \rangle$ decreases rapidly while the parent polymers are breaking. After this, the slower scission rates of the daughter polymers lead to a more gradual decrease in $\langle Wi \rangle$, which eventually will saturate to a value less than Wi_{cr}, corresponding to daughter polymers that cannot be broken up further by the flow. This effect cannot be captured by dumbbells, which directly break into beads (figure 8).

The reduction of $\langle Wi \rangle$ with time has a strong influence on the evolution of the mean end-to-end extension of the polymers $\langle R \rangle$, as shown in figure 12(c). After an initial stretching phase, $\langle R \rangle$ begins to decrease, owing to both the scission of highly stretched polymers and the smaller Wi of the resulting daughter polymers. After all scissions cease, we are left with relatively inextensible daughter polymers whose extensions fluctuate near r_{eq}. Interestingly, the curve for $Wi_0 = 2.0$ shows two regimes in the decay of $\langle R \rangle$. The first fast-decay regime is due to the rapid scission of 10-bead parents (see figure 11c); the second slow-decay regime results from the much slower breakup of 5-bead daughter polymers, for which $Wi = 0.55$ barely satisfies the condition for secondary scission ($Wi > Wi_{cr} = 1/2$). This second slow regime is not seen for either smaller or larger Wi_0: in the former case, secondary breakups do not occur, whereas in the latter case secondary breakups occur very quickly (see figure 11).

5. Concluding remarks

Polymers, even in small quantities, have a dramatic impact on a turbulent flow, reducing drag or dissipation and suppressing small-scale motion. However, because these effects originate from polymer stretching (and the resultant feedback forces), the polymers which exert the strongest influence on the flow are also the most susceptible to strain-induced scission. Therefore, to achieve effective flow modification, one must strike a balance between these opposing tendencies, which in turn demands a detailed understanding of the scission process and the factors that influence the rate of scission.

In this work, we have analysed the scission of polymers in homogeneous isotropic turbulence, with a focus on the temporal decay of unbroken polymers, and the statistics of their survival times. By using DNS, we have quantified the decay time (or scission rate) as a function of Wi, which can serve as inputs for coarse-grained models. Importantly, all the key qualitative features of the numerical results can be predicted analytically by replacing the fluctuating, turbulent velocity gradient by a time-decorrelated Gaussian random flow. This is possible because scission is caused by the cumulative action of fluctuating strain, and not by sudden stretching in high-strain regions of the flow.

The scission statistics have been shown to be qualitatively insensitive to the strength of HI and EV interactions among the beads of the polymer chain model. Quantitatively, these two interactions have opposing effects, with hydrodynamic (EV) interactions suppressing (enhancing) the scission rate by delaying (hastening) the uncoiling of coiled polymer chains. Another finding, relevant for future computations, is that a multibead polymer chain cannot be replaced by a dumbbell model without incurring quantitative errors in the prediction of breakup rates. However, the results appear to converge as N_b increases, so we expect $N_b \sim O(10)$ to be sufficient even if a polymer model may strictly demand many more beads.

Our study of the scission of active polymers has shown that there is an intermediate value of Wi for which the overall, time-integrated, reduction of the kinetic energy dissipation rate is maximum: for small Wi the polymers do not stretch and the feedback is weak, whereas for large Wi the stretching and feedback is initially strong, but the resultant dissipation reduction is lost rapidly as the polymers break up very quickly. This study also demonstrates the usefulness of the hybrid Eulerian–Lagrangian method for the simulation of scission in turbulent polymer solutions. This approach indeed directly applies a suitable scission criterion to individual polymer molecules instead of modelling the effect of scission on the polymer-conformation tensor field. In the hybrid simulations presented here, the description of the polymer phase was necessarily restricted to the elastic-dumbbell model, because a very large ensemble of molecules is required to obtain an appreciable feedback on the flow. However, it is hoped that in future it will possible to use more refined polymer models.

We have shown that in a sufficiently strong turbulent flow (large Wi) polymers can break up repeatedly. However, because the fragments in each successive generation have a smaller relaxation time, the breakup process eventually ceases once the effective Wi of the surviving polymer fragments becomes less than Wi_{cr}. From this condition, we can estimate the number of beads in the largest surviving chains as $\mathscr{N}(\mathscr{N}+1) \leqslant 6Wi_{cr}\tau_\eta/\tau$ (using (3.17*a*)). Now, as $\mathscr{N}$ is linearly related to the mass of a polymer, this condition allows us to estimate how the weight-averaged molar mass (biased towards the largest chains) of the surviving polymers M_{ws} scales with the Reynolds number Re. For large $\mathscr{N}$, we have $\mathscr{N}^2 \sim \tau_\eta/\tau \sim Re^{-3/2}\nu_f/D^2\tau$, where D is the large length scale of the flow system. Therefore, for a specified polymer, solvent and system geometry we obtain $M_{ws}^2 \sim Re^{-3/2}$. This scaling is consistent with the experimental data of Vanapalli *et al.* (2006), who obtain a power-law exponent close to $-3/2$ for a variety of polymers and system geometries (these results are reported in terms of the squared, weight-averaged polymer length which is linearly related to M_{ws}^2, as described in the data analysis section of Vanapalli *et al.* (2006)). The same scaling was extended to higher Reynolds numbers by Elbing *et al.* (2009).

The flow of a polymer solution in the elastic-turbulence regime shares many similarities with the viscous range of Newtonian turbulence (Steinberg 2009). However, the above argument for estimating M_{ws} cannot be easily adapted to elastic turbulence, because the amplitude of the fluctuating strain rate decays along with the concentration of unbroken polymers. Thus, M_{ws} depends on the time evolution of the chaotic flow, which is not known *a priori*.

The multiple-scission statistics of a polymer also show a non-monotonic dependence on Wi. Small Wi polymers break only once, if at all, whereas large Wi polymers undergo a rapid succession of breakups and quickly reach their limiting generation (fragments which are no longer stretched by the flow). However, for intermediate Wi, the first-scission occurs quickly, but then the daughter polymers break up much more slowly. This introduces multiple time scales into the decay of $\langle Wi\rangle$, the average effective Wi of the polymer population. This average quantity and its evolution are relevant to coarse-grained continuum models of polymer solutions which typically contain a single mean polymer-relaxation-time parameter. Indeed, the development of continuum models that incorporate scission is essential for predicting the long-time dynamics of turbulent polymer solutions in complex applications. The quantitative results as well as physical insights gained from this study should aid in the development of such models.

Finally, the present study is based on a coarse-grained description of a polymer molecule and of the scission process. In the context of laminar flows, a fine-grained model of polymer scission has been proposed by Sim *et al.* (2007). Here, the polymer is modelled by

a chain of a large number of beads joined by rigid rods, which more faithfully represents the entropic coiling process than a bead-spring model. Scission is based on the tension exerted by the flow on the rods, but is implemented as a stochastic event, respecting the stochasticity of both covalent bond breakup and the fluctuating rod-tension. We hope that with future increases in computational power, it will become possible to use such fine-grained polymer models in Lagrangian simulations of polymers in turbulent flows and thus reach a deeper understanding of the scission process.

Acknowledgements. The computations were performed at Centre de Calculs Interactifs of Université Côte d'Azur, at Information Technology Centre in Nagoya University and National Institute for Fusion Science (NIFS), at the cluster Mowgli and the work station Goopy at the ICTS–TIFR, and at the workstation Aragorn at IIT Bombay.

Funding. J.R.P., S.S.R. and D.V. thank the Indo–French Centre for Applied Mathematics (IFCAM) for financial support. D.V. acknowledges his Associateship with the International Centre for Theoretical Sciences, Tata Institute of Fundamental Research, Bangalore, India. T.W. acknowledges the financial support by MEXT KAKENHI through grant no. 20H00225 and JSPS KAKENHI (grant no. 18K03925), and the computational supports provided by JHPCN (jh190018-NAH, jh200006) and by NIFS (NIFS18KNXN366, NIFS18KNSS105). S.S.R. acknowledges support of the DAE, Government of India, under project no. 12-R&D-TFR-5.10-1100 as well as the DST (India) projects MTR/2019/001553 and ECR/2015/000361 for support. J.R.P. acknowledges funding from the IIT Bombay IRCC Seed grant.

Declaration of interests. The authors report no conflict of interest.

Author ORCIDs.
Dario Vincenzi https://orcid.org/0000-0003-3332-3802;
Takeshi Watanabe https://orcid.org/0000-0003-2503-6782;
Samriddhi Sankar Ray https://orcid.org/0000-0001-9407-0007;
Jason R. Picardo https://orcid.org/0000-0002-9227-5516.

Appendix A

In this appendix, we present a modified version of the bead-chain model (§ 2) that takes into account HI, using the Rotne–Prager–Yamakawa mobility tensor, and implements EV interactions using a repulsive, narrow Gaussian potential. We follow the formulation given in Schroeder *et al.* (2004), but rewrite the equations in terms of the notation and parameters of § 2. The equation for the motion of the centre of mass remains the same as (2.1*a*). The evolution of the separation vectors $\boldsymbol{Q}_i$, however, is now governed by

$$\dot{\boldsymbol{Q}}_i = \boldsymbol{\kappa}(t)\cdot\boldsymbol{Q}_i + \frac{1}{4\tau}\sum_{j=1}^{\mathscr{N}}\left(\boldsymbol{D}_{i+1,j}-\boldsymbol{D}_{i,j}\right)\cdot\left(\boldsymbol{F}_j^E-\boldsymbol{F}_j^{EV}\right) + \sqrt{\frac{Q_{eq}^2}{6\tau}}\sum_{j=1}^{i+1}\left(\boldsymbol{B}_{i+1,j}-\boldsymbol{B}_{i,j}\right)\cdot\boldsymbol{\xi}_j(t), \quad i=1,\ldots,\mathscr{N}-1. \tag{A1}$$

Here, $\boldsymbol{F}_i^E = f_i\boldsymbol{Q}_i - f_{i-1}\boldsymbol{Q}_{i-1}$ is the net FENE spring force exerted on bead i, with the coefficients f_i still given by (2.2) ($\boldsymbol{Q}_0$ and $\boldsymbol{Q}_{\mathscr{N}}$ must be replaced by zero to obtain the forces on the first and last bead, respectively). The net force due to EV interactions acting on bead i, $\boldsymbol{F}_i^{EV}$, is given by

$$\boldsymbol{F}_i^{EV} = -\sum_{j=1;j\neq i}^{\mathscr{N}} \nu\frac{3^4}{2^{5/2}\pi^{3/2}}\left(\frac{Q_m}{Q_{eq}}\right)^4\exp\left(-\frac{9}{2}\frac{X_{ij}^2}{Q_{eq}^2}\right)\boldsymbol{X}_{ij}, \tag{A2}$$

where ν is a non-dimensional parameter that sets the magnitude of the EV forces, $\boldsymbol{X}_i$ is the position vector of bead i, $\boldsymbol{X}_{ij} = \boldsymbol{X}_j - \boldsymbol{X}_i$ is the displacement vector between beads i and j, and $X_{ij} = |\boldsymbol{X}_{ij}|$. The Rotne–Prager–Yamakawa mobility tensor $\boldsymbol{D}_{i,j}$ is given by

$$\boldsymbol{D}_{i,j} = \boldsymbol{I} \quad \text{if } i = j, \tag{A3}$$

$$\boldsymbol{D}_{i,j} = \frac{6a}{8X_{ij}}\left[\left(1 + \frac{2a^2}{3X_{ij}^2}\right)\boldsymbol{I} + \left(1 - \frac{2a^2}{X_{ij}^2}\right)\frac{\boldsymbol{X}_{ij}\boldsymbol{X}_{ij}}{X_{ij}^2}\right] \quad \text{if } i \neq j \text{ and } X_{ij} \geqslant 2a, \tag{A4}$$

$$\boldsymbol{D}_{i,j} = \left[\left(1 - \frac{9X_{ij}}{32a}\right)\boldsymbol{I} + \frac{3}{32}\frac{\boldsymbol{X}_{ij}\boldsymbol{X}_{ij}}{aX_{ij}}\right] \quad \text{if } i \neq j \text{ and } X_{ij} < 2a, \tag{A5}$$

where $\boldsymbol{I}$ is the 3×3 identity tensor and a is the radius of the beads, which defines the non-dimensional HI parameter

$$h = \frac{a}{Q_{eq}}\left(\frac{3}{\pi}\right)^{1/2}. \tag{A6}$$

This definition implies that physically meaningful values of h should be $\lesssim 1/2$ (Schroeder *et al.* 2004).

Finally, the coefficient matrix $\boldsymbol{B}_{i,j}$ is related to the positive definite mobility tensor by

$$\boldsymbol{D}_{i,j} = \sum_{l=1}^{\mathscr{N}} \boldsymbol{B}_{i,l} \cdot \boldsymbol{B}_{j,l}^{\mathrm{T}}, \tag{A7}$$

where the superscript T denotes the transpose. To compute $\boldsymbol{B}_{i,j}$, we first combine the $\mathscr{N}^2$ different $\boldsymbol{D}_{i,j}$ matrices into a $3\mathscr{N} \times 3\mathscr{N}$ block matrix, and then carry out a Cholesky decomposition to obtain a lower triangular block matrix that yields the $\boldsymbol{B}_{i,j}$ matrices (Jendrejack *et al.* 2002). Note that $\boldsymbol{B}_{i,j} = 0$ if $j > i$.

Equations (A1) to (A7), along with (2.1*a*), constitute the bead-spring chain model with HI and EV interactions, the magnitudes of which are set by the two new parameters h and ν, respectively, such that substituting $h = \nu = 0$ yields the Rouse model of § 2.

References

Allende, S., Henry, C. & Bec, J. 2020 Dynamics and fragmentation of small inextensible fibers in turbulence. *Phil. Trans. R. Soc. Lond.* A **378**, 20190398.

Balkovsky, E., Fouxon, A. & Lebedev, V. 2000 Turbulent dynamics of polymer solutions. *Phys. Rev. Lett.* **84**, 4765–4768.

Bec, J., Biferale, L., Boffetta, G., Cencini, M., Lanotte, A., Musacchio, S. & Toschi, F. 2006 Lyapunov exponents of heavy particles in turbulence. *Phys. Fluids* **18**, 091702.

Benzi, R. 2010 A short review on drag reduction by polymers in wall bounded turbulence. *Physica* D **239**, 1338–1345.

Biferale, L., Meneveau, C. & Verzicco, R. 2014 Deformation statistics of sub-Kolmogorov-scale ellipsoidal neutrally buoyant drops in isotropic turbulence. *J. Fluid Mech.* **754**, 184–207.

Bird, R.B., Curtiss, C.F., Armstrong, R.C. & Hassager, O. 1977 *Dynamics of Polymeric Liquids*, vol. II. Wiley.

Bird, R.B., Dotson, P.J. & Johnson, N.L. 1980 Polymer solution rheology based on a finitely extensible bead–spring chain model. *J. Non-Newtonian Fluid Mech.* **7**, 213–235.

Cascales, J.J.L. & de la Torre, J.G. 1991 Simulation of polymer chains in elongational flow. Steady-state properties and chain fracture. *J. Chem. Phys.* **95**, 9384–9392.

CASCALES, J.J.L. & DE LA TORRE, J.G., 1992 Simulation of polymer chains in elongational flow. Kinetics of chain fracture and fragment distribution. *J. Chem. Phys.* **97**, 4549–4554.

CELANI, A., MUSACCHIO, S. & VINCENZI, D. 2005 Polymer transport in random flow. *J. Stat. Phys.* **118**, 531–554.

DE CHAUMONT QUITRY, A. & OUELLETTE, N.T. 2016 Concentration effects on turbulence in dilute polymer solutions far from walls. *Phys. Rev.* E **93**, 063116.

CHERTKOV, M. 2000 Polymer stretching by turbulence. *Phys. Rev. Lett.* **84**, 4761–4764.

CHOI, H.J., LIM, S.T., LAI, P.-Y. & CHAN, C.K., 2002 Turbulent drag reduction and degradation of DNA. *Phys. Rev. Lett.* **89**, 088302.

CIFRE, J.G.H. & DE LA TORRE, J.G. 1999 Steady-state behavior of dilute polymers in elongational flow. Dependence of the critical elongational rate on chain length, hydrodynamic interaction, and excluded volume. *J. Rheol.* **43**, 339.

CRAWFORD, A.M., MORDANT, N., XU, H. & BODENSCHATZ, E. 2008 Fluid acceleration in the bulk turbulence of dilute polymer solutions. *New J. Phys.* **10**, 123015.

DE ANGELIS, E., CASCIOLA, C.M., BENZI, R. & PIVA, R. 2005 Homogeneous isotropic turbulence in dilute polymers. *J. Fluid Mech.* **531**, 1–10.

ELBING, B.R., WINKEL, S., SOLOMON, J. & CECCIO, L. 2009 Degradation of homogeneous polymer solutions in high shear turbulent pipe flow. *Exp. Fluids* **47**, 1033–1044.

FALKOVICH, G., GAWĘDZKI, K. & VERGASSOLA, M. 2001 Particles and fields in fluid turbulence. *Rev. Mod. Phys.* **73**, 913–975.

GIRIMAJI, S.S. & POPE, S.B. 1990 A diffusion model for velocity gradients in turbulence. *Phys. Fluids* A **2**, 242–256.

GRAHAM, M.D. 2014 Drag reduction and the dynamics of turbulence in simple and complex fluids. *Phys. Fluids* **26**, 101301.

GROISMAN, A. & STEINBERG, V. 2004 Elastic turbulence in curvilinear flows of polymer solutions. *New J. Phys.* **6**, 29.

HORN, A.F. & MERRILL, E.W. 1984 Midpoint scission of macromolecules in dilute solution in turbulent flow. *Nature* **312**, 140–141.

HSIEH, C.C., PARK, S.J. & LARSON, R.G. 2005 Brownian Dynamics modeling of flow-induced birefringence and chain scission in dilute polymer solutions in a planar cross-slot flow. *Macromolecules* **38**, 1456–1468.

JENDREJACK, R.M., DE PABLO, J.J. & GRAHAM, M.D. 2002 Stochastic simulations of DNA in flow: dynamics and the effects of hydrodynamic interactions. *J. Chem. Phys.* **116**, 7752.

JIN, S. & COLLINS, L.R. 2008 Dynamics of dissolved polymer chains in isotropic turbulence. *New J. Phys.* **9**, 360.

KALELKAR, C., GOVINDARAJAN, R. & PANDIT, R. 2005 Drag reduction by polymer additives in decaying turbulence. *Phys. Rev.* E **72**, 017301.

KNUDSEN, K.D., HERNÁNDEZ CIFRE, J.G. & GARCÍA DE LA TORRE, J. 1996 Conformation and fracture of polystyrene chains in extensional flow studied by numerical simulation. *Macromolecules* **29**, 3603–3610.

KRAICHNAN, R.H. 1968 Small-scale structure of a scalar field convected by turbulence. *Phys. Fluids* **11**, 945–953.

LARSON, R.G. 1999 *The Structure and Rheology of Complex Fluids*. Oxford University.

LIU, Y. & STEINBERG, V. 2014 Single polymer dynamics in a random flow. *Macromol. Symp.* **337**, 34–43.

LUMLEY, J.L. 1972 On the solution of equations describing small scale deformation. In *Symposia Mathematica, Istituto Nazionale di Alta Matematica, Bologna*, vol. IX, pp. 315–334. Academic Press.

MOUSSA, T., TIU, C. & SRIDHAR, T. 1993 Effect of solvent on polymer degradation in turbulent flow. *J. Non-Newtonian Fluid Mech.* **48**, 261–284.

MUSACCHIO, S. & VINCENZI, D. 2011 Deformation of a flexible polymer in a random flow with long correlation time. *J. Fluid Mech.* **670**, 326–336.

OLDROYD, D.J. 1950 On the formulation of rheological equations of state. *Proc. R. Soc. Lond.* A **200**, 523–541.

ÖTTINGER, H.C. 1996 *Stochastic Processes in Polymeric Fluids*. Springer.

OUELLETTE, N.T., XU, H. & BODENSCHATZ, E. 2009 Bulk turbulence in dilute polymer solutions. *J. Fluid Mech.* **629**, 375–385.

OWOLABI, B.E., DENNIS, D.J.C. & POOLE, R.J. 2017 Turbulent drag reduction by polymer additives in parallel-shear flows. *J. Fluid Mech.* **827**, R4.

PATERSON, R.W. & ABERNATHY, F.H. 1970 Turbulent flow drag reduction and degradation with dilute polymer solutions. *J. Fluid Mech.* **43**, 689–710.

PEREIRA, A.S. & SOARES, E.J. 2012 Polymer degradation of dilute solutions in turbulent drag reducing flows in a cylindrical double gap rheometer device. *J. Non-Newtonian Fluid Mech.* **179-180**, 9–22.

PEREIRA, A.S., MOMPEAN, G. & SOARES, E.J. 2018 Modeling and numerical simulations of polymer degradation in a drag reducing plane Couette flow. *J. Non-Newtonian Fluid Mech.* **256**, 1–7.

PERKINS, T.T., SMITH, D.E. & CHU, S. 1997 Single polymer dynamics in an elongational flow. *Science* **276**, 2016–2021.

PERLEKAR, P., MITRA, D. & PANDIT, R. 2006 Manifestations of drag reduction by polymer additives in decaying, homogeneous, isotropic turbulence. *Phys. Rev. Lett.* **97**, 264501.

PERLEKAR, P., MITRA, D. & PANDIT, R. 2010 Direct numerical simulations of statistically steady, homogeneous, isotropic fluid turbulence with polymer additives. *Phys. Rev.* E **82**, 066313.

PLAN, E.L.C.VI.M., ALI, A. & VINCENZI, D. 2016 Bead-rod-spring models in random flows. *Phys. Rev.* E **94**, 020501(R).

POOLE, R.J. 2020 Editorial for the special issue on 'Polymer degradation in turbulent drag reduction'. *J. Non-Newtonian Fluid Mech.* **281**, 104283.

PROCACCIA, I., L'VOV, V.S. & BENZI, R. 2008 Theory of drag reduction by polymers in wall-bounded turbulence. *Rev. Mod. Phys.* **80**, 225–247.

RAY, S.S. & VINCENZI, D. 2018 Droplets in isotropic turbulence: deformation and breakup statistics. *J. Fluid Mech.* **852**, 313–328.

ROUSE, P.E. 1953 A theory of the linear viscoelastic properties of dilute solutions of coiling polymers. *J. Chem. Phys.* **21**, 1272–1280.

SCHROEDER, C.M., SHAQFEH, E.S.G. & CHU, S. 2004 Effect of hydrodynamic interactions on DNA dynamics in extensional flow: simulation and single molecule experiment. *Macromolecules* **37**, 9242–9256.

SIM, H.G., KHOMAMI, B. & SURESHKUMAR, R. 2007 Flow-induced chain scission in dilute polymer solutions: algorithm development and results for scission dynamics in elongational flow. *J. Rheol.* **51**, 1223–1251.

SOARES, E.J. 2020 Review of mechanical degradation and de-aggregation of drag reducing polymers in turbulent flows. *J. Non-Newtonian Fluid Mech.* **276**, 104225.

STONE, P.A. & GRAHAM, M.D. 2003 Polymer dynamics in a model of the turbulent buffer layer Phys. *Fluids* **15**, 1247–1256.

STEINBERG, V. 2009 Elastic stresses in random flow of a dilute polymer solution and the turbulent drag reduction problem. *C. R. Phys.* **10**, 728–738.

THIFFEAULT, J.-L. 2003 Finite extension of polymers in turbulent flow. *Phys. Lett.* A **308**, 445–450.

TOMS, B.A. 1949 Some observations on the flow of linear polymer solutions through straight tubes at large Reynolds numbers. In *Proceedings of the First International Congress on Rheology, North-Holland, Amsterdam*, vol. II, pp. 135–141. North-Holland Publishing Company.

TOMS, B.A. 1977 On the early experiments on drag reduction by polymers. *Phys. Fluids* **20**, S3–S5.

DEN TOONDER, J.M.J., DRAAD, A.A., KUIKEN, G.D.C. & NIEUWSTADT, F.T.M. 1995 Degradation effects of dilute polymer solutions on turbulent drag reduction in pipe flows. *Appl. Sci. Res.* **55**, 63–82.

VANAPALLI, S.A., ISLAM, M.T. & SOLOMON, M.J. 2005 Scission-induced bounds on maximum polymer drag reduction in turbulent flow. *Phys. Fluids* **17**, 095108.

VANAPALLI, S.A., CECCIO, S.L. & SOLOMON, M.J. 2006 Universal scaling for polymer chain scission in turbulence. *Proc. Natl Acad. Sci. USA* **103**, 16660–16665.

VILLERMAUX, E. 2007 Fragmentation. *Annu. Rev. Fluid Mech.* **39**, 419–446.

VILLERMAUX, E. 2020 Fragmentation versus cohesion. *J. Fluid Mech.* **898**, P1.

VAITHIANATHAN, T. & COLLINS, L.R. 2003 Numerical approach to simulating turbulent flow of a viscoelastic polymer solution. *J. Comput. Phys.* **187**, 1–21.

VINCENZI, D., JIN, S., BODENSCHATZ, E. & COLLINS, L.R. 2007 Stretching of polymers in isotropic turbulence: a statistical closure. *Phys. Rev. Lett.* **98**, 024503.

VINCENZI, D., PERLEKAR, P., BIFERALE, L. & TOSCHI, F. 2015 Impact of the Peterlin approximation on polymer dynamics in turbulent flows. *Phys. Rev.* E **92**, 053004.

VIRK, P.S. 1975 Drag reduction fundamentals. *AIChE J.* **21**, 625–656.

WATANABE, T. & GOTOH, T. 2010 Coil-stretch transition in an ensemble of polymers in isotropic turbulence. *Phys. Rev.* E **81**, 066301.

WATANABE, T. & GOTOH, T. 2013*a* Hybrid Eulerian–Lagrangian simulations for polymer-turbulence interactions. *J. Fluid Mech.* **717**, 535–575.

WATANABE, T. & GOTOH, T. 2013*b* Kinetic energy spectrum of low-Reynolds-number turbulence with polymer additives. *J. Phys.: Conf. Ser.* **454**, 012007.

WATANABE, T. & GOTOH, T. 2014 Power-law spectra formed by stretching polymers in decaying isotropic turbulence. *Phys. Fluids* **26**, 035110.

WHITE, C.M. & MUNGAL, M.G. 2008 Mechanics and prediction of turbulent drag reduction with polymer additives. *Annu. Rev. Fluid Mech.* **40**, 235–256.

WU, S., LI, C., ZHENG, Q. & XU, L. 2018 Modelling DNA extension and fragmentation in contractive microfluidic devices: a Brownian dynamics and computational fluid dynamics approach. *Soft Matt.* **14**, 8780–8791.

XI, H.-D., BODENSCHATZ, E. & XU, H. 2013 Elastic energy flux by flexible polymers in fluid turbulence. *Phys. Rev. Lett.* **111**, 024501.

YEUNG, P.K. 2002 Lagrangian investigations of turbulence. *Annu. Rev. Fluid Mech.* **34**, 115–142.